1-1-2005

Development Of An Improved On-Line Voltage Stability Index Using Synchronized Phasor Measurement

Yanfeng Gong

DEVELOPMENT OF AN IMPROVED ON-LINE VOLTAGE STABILITY INDEX USING SYNCHRONIZED PHASOR MEASUREMENT

By

Yanfeng Gong

A Dissertation
Submitted to the Faculty of
Mississippi State University
in Partial Fulfillment of the Requirements
for the Degree of Doctor of Philosophy
in Electrical Engineering
in the Department of Electrical and Computer Engineering

Mississippi State, Mississippi

December 2005

DEVELOPMENT OF AN IMPROVED ON-LINE VOLTAGE STABILITY

INDEX USING SYNCHRONIZED PHASOR MEASUREMENT

By

Yanfeng Gong

Approved:

Noel N. Schulz Associate Professor of Electrical and Computer Engineering (Major Professor and Director of Dissertation)	Justin S. Davis Assistant Professor of Electrical and Computer Engineering (Committee Member)
Randolph F. Follett Assistant Professor of Electrical and Computer Engineering (Committee Member)	Herbert L. Ginn III Assistant Professor of Electrical and Computer Engineering (Committee Member)
Nicholas H. Younan Professor of Electrical and Computer Engineering (Graduate Coordinator)	Kirk H. Schulz Dean of the College of Engineering

Name: Yanfeng Gong

Date of Degree: December 10, 2005

Institution: Mississippi State University

Major Field: Electrical Engineering

Major Professor: Noel N. Schulz

Title of Study: DEVELOPMENT OF AN IMPROVED ON-LINE VOLTAGE STABILITY INDEX USING SYNCHRONIZED PHASOR MEASUREMENT

Pages in Study: 110

Candidate for Degree of Doctor of Philosophy

Recent events, such as the Northeast Blackout of 2003, have highlighted the need for accurate real-time stability assessment techniques to detect when an electric power system is on the brink of voltage collapse. While many techniques exist, most techniques are computationally demanding and cannot be used in an on-line application. A voltage stability index (VSI) can be designed to estimate the distance of the current operating point to the voltage marginally stable point during the system operation. In this research work, a new VSI was developed that not only can detect the system voltage marginally stable point but also is computationally efficient for on-line applications. Starting with deriving a method to predict three types of maximum transferable power of a single source power system, the new VSI is based on the three calculated load margins. In order to apply the VSI to large power systems, a method has been developed to simplify the large network behind a load bus into a single source and a single transmission line given the synchronized phasor measurements of the power system variables and network

parameters. The simplified system model, to which the developed VSI can be applied, preserves the power flow and the voltage of the particular load bus. The proposed voltage stability assessment method, therefore, provides a VSI of each individual load bus and can identify the load bus that is the most vulnerable to voltage collapse. Finally, the new VSI was tested on three power systems. Results from these three test cases provided validation of the applicability and accuracy of the proposed VSI.

DEDICATION

I would like to dedicate this dissertation to my parents.

ACKNOWLEDGMENTS

I would like to express my sincere gratitude to my advisor, Dr. Noel N. Schulz, for her assistance, encouragement and generosity during my studies at Mississippi State University and Michigan Technological University. Many thanks to Dr. Schulz for enlightening me not only in conducting academic research but also in many other ways.

Thanks are also due to Dr. Justin Davis, Dr. Herb Ginn, and Dr. Randy Follett for serving as members of my committee.

I gratefully acknowledge the financial support of the Office of Navy Research (ONR) and Schweitzer Engineering Laboratories (SEL) during my Ph.D. studies.

I also convey thanks to Armando Guzmán at SEL for his insightful discussions on this research subject and Normann Fischer at SEL for teaching me to be a good engineer.

Finally I would like to express my deepest appreciation to my parents and wife for their love, support and encouragement throughout the years I have been studying aboard.

TABLE OF CONTENTS

Page

DEDICATION ii

ACKNOWLEDGMENTS iii

LIST OF TABLES vii

LIST OF FIGURES viii

CHAPTER

I. INTRODUCTION 1

1.1 Introduction 1
1.2 Objectives of the dissertation 4
1.3 Outline of the dissertation 5

II. VOLTAGE STABILITY PROBLEM 7

2.1 Introduction 7
2.2 Definition and classification of voltage stability 10
2.2.1 Definition of voltage stability 10
2.2.2 Classification of voltage stability 12
2.3 Voltage collapse mechanism 15
2.3.1 Power system load 15
2.3.2 Line power transmission capacity 20
2.3.3 Power generation capacity 24
2.3.4 A simple example to illustrate the voltage instability 28
2.4 Summary 33

III. LITERATURE REVIEW OF VOLTAGE STABILITY ASSESSMENT METHODS 34

3.1 Power system dynamic modeling and simulation 34
3.2 Steady-state analysis 37
3.2.1 Power flow analysis 37
3.2.2 PV/VQ curve and continuation power flow 39

CHAPTER Page

3.3 Voltage stability indices 41
3.3.1 Singular values and eigenvalues of Jacobian matrix 42
3.3.2 Sensitivity factors 44
3.3.3 Existence of multiple power flow solutions 46
3.3.4 Load flow feasibility 47
3.3.5 Thevenin equivalent impedance 48
3.3.6 Load margin 49
3.3.7 Voltage 50
3.3.8 Power system reactive power reserve 51
3.4 Summary 52

IV. STATEMENT OF PROBLEM AND WORK PLAN 53

4.1 Introduction 53
4.2 Limitation of existing indices 53
4.2.1 Power flow related indices 53
4.2.2 Direct measurement based indices 55
4.3 Synchronized phasor measurement 56
4.4 Motivation 57
4.5 Work plan 58

V. IMPROVED VOLTAGE STABILITY INDEX DEVELOPMENT 60

5.1 Introduction 60
5.2 Voltage stability index for simple power system 61
5.2.1 Maximum transferable power through a transmission line 61
5.2.2 Load margins of the single line system 65
5.2.3 Voltage stability indices of single line system 70
5.3 Voltage stability index of a large power system 71
5.3.1 Power system partition 71
5.3.2 Power system network simplification 73
5.3.3 Large margin and VSI of a large power system 78
5.4 Measurement requirements for the proposed VSI 79
5.5 Practical implementation of the VSI 79
5.6 Summary 80

VI. PROPOSED VSI APPLICATION IN POWER SYSTEMS 82

6.1 Introduction 82
6.2 BPA 10-bus test system 83
6.2.2 Steady state power flow analysis 84
6.2.3 Time based dynamic simulation 87
6.3 IEEE 30-bus test system 92
6.3.2 Increase an individual load 93

CHAPTER Page

6.3.3 Increase all loads simultaneously 95
6.4 CIGRE 32-bus test system 97
6.5 Results, analysis and discussion 100
6.6 Summary 102

VII. CONCLUSIONS AND FUTURE WORK 103

7.1 Conclusions 103
7.2 Future work 104

REFERENCES 106

LIST OF TABLES

TABLE		Page
1.1	Voltage instable incidents [2]	2
2.1	Exponents of different loads [3]	17
2.2	Typical parameter values for generic load model [13]	19
3.1	Dynamic model equations for the 4-bus example system [3]	36
3.2	Under-voltage load shedding scheme example [46]	50
6.1	Generator capacity limits of the BPA 10-bus system	84
6.2	BPA test system bus voltages in p.u. (before and after line outage)	85
6.3	VSI outputs of the BPA test system based on steady state analysis	86
6.4	Five load buses with the minimum VSI under the initial condition	92
6.5	VSI computation time	102

LIST OF FIGURES

FIGURE Page

2.1 Classification of power system stability problems [4] 8

2.2 Time frame for voltage stability phenomena [2] 14

2.3 Simplified generic dynamic load model 18

2.4 Load dynamics illustration 20

2.5 A two-bus power system model 21

2.6 Three-dimensional plot of *PQV* (View from front) 23

2.7 Three-dimensional plot of *PQV* (View from side) 23

2.8 Transferable PQ power 24

2.9 Steady-state equivalent circuit of a synchronous generator [4] 26

2.10 A three-bus power system to illustrate the voltage instability 29

2.11 Steady state analysis results of the simple power system 31

2.12 Load active power P versus time for Figure 2.10 32

2.13 Load voltage V_r versus time for Figure 2.10 32

2.14 Load voltage V_r vs. load reactive power P for Figure 2.10 33

3.1 A four-bus power system [3] 36

3.2 PV curves of the two-bus power system as shown in Figure 2.5 40

3.3 Thevenin equivalent circuit 48

4.1 Voltage stability indices classification 54

FIGURE Page

4.2 General structure of PMU [6] 57

5.1 Single line power system model 61

5.2 Maximum transferable active power P_{max} vs. reactive power Q 64

5.3 Maximum transferable reactive power Q_{max} vs. active power P 64

5.4 Maximum transferable complex power S_{max} vs. load power factor α 64

5.5 Predicted P_{max} vs. P for system in Example 5.1 67

5.6 Predicted Q_{max} vs. Q for system in Example 5.1 68

5.7 Predicted S_{max} vs. S for system in Example 5.1 68

5.8 Possible load voltage Vr for the system in Example 5.1 69

5.9 Three predicted load margins of the system in Example 5.1 69

5.10 Voltage stability indices for the system in Example 5.1 70

5.11 Interconnected power system 71

5.12 Equivalent interconnected power system (extended Ward method) 72

5.13 Equivalent interconnected power system (PV bus) 73

5.14 Derived equivalent single source power system 76

5.15 A three-bus power system of Example 5.2 77

5.16 Functional diagram of the proposed VSI implementation 81

6.1 BPA 10-bus test system one-line diagram [2] 83

6.2 Proposed VSI of the BPA test system (from steady state analysis) 86

6.3 Bus voltages of BPA test system (from steady state analysis) 87

6.4 Load bus 7 load margin and VSI (from dynamic simulation) 89

6.5 Load bus 10 load margin and VSI (from dynamic simulation) 90

6.6 VSI of the BPA ten-bus system (from dynamic simulation) 91

FIGURE Page

6.7 Bus voltages of BPA ten-bus system (from dynamic simulation) 91

6.8 IEEE 30-bus test system one-line diagram [57] 93

6.9 VSIs of selected load buses 94

6.10 Predicted S_{max} of load bus 10 95

6.11 The five buses with the minimum VSIs (loads increased evenly) 96

6.12 Predicted S_{max} of bus 30 (loads increased evenly) 96

6.13 CIGRE 32-bus test system one-line diagram 98

6.14 VSIs of the CIGRE 32-bus system 99

CHAPTER I

INTRODUCTION

1.1 Introduction

Voltage collapse or instability is emerging as a major concern to utility companies to maintain a stable power system operation as power system construction and operation practices have undergone substantial transformation over the past two decades. Factors that contribute to the voltage instability include the following:

- The average increase in system loads has been steadily surpassing the construction of new power system infrastructure, including power plants and transmission lines. Power systems are being operated closer to their security and stability limits.
- The expansion of the transmission network is severely limited by environmental constraints. Increasing the reactive power compensation is chosen by utilities as an alternative solution to building new transmission lines.
- Long distance bulk power transfers have become ordinary under the deregulation incentives.
- System operations are increasingly automated and fewer personnel are engaging in the supervision and operation of power systems.

Voltage instability has caused several major power system collapses around the world. Table 1.1 lists a few major voltage instability incidents up to 1994. Voltage instability also partially contributed to several other recent major blackouts including the recent Northeastern US blackout that happened on August 14, 2003. Investigation results [1] of the August 2003 blackout have revealed that the blackout could have been prevented if proper automatic under voltage load shedding schemes had been placed at certain areas.

Table 1.1 Voltage instable incidents [2]

Date	Location	Time Frame
December 1, 1987	Western France	4-6 minutes
August 22, 1987	Western Tennessee	10 seconds
July 23, 1987	Tokyo, Japan	20 minutes
November 30, 1986	SE Brazil, Paraguay	2 seconds
December 27, 1983	Sweden	55 seconds
December 30, 1982	Florida	1-3 minutes
August 4, 1982	Belgium	4.5 minutes
December 19, 1978	France	26 minutes
August 22, 1970	Japan	30 minutes

Since the voltage instability issue started to emerge, significant research efforts from the power engineering community have been devoted to studying the voltage instability mechanism and to developing analysis tools and control schemes to mitigate the instability. Two monographs [2,3] and an individual book chapter of a textbook [4] have been devoted to this topic as well as numerous technical papers and reports. This literature has demonstrated that a good understanding of the voltage instability mechanism has been achieved. Meanwhile, many researchers agree that the voltage instability problem is a high order nonlinear problem as a large number of different types

of devices are involved in the voltage dynamics. Also a wide variety of modeling and simulation principles and analysis and control methods of the power system voltage stability have been developed.

In general these voltage stability analysis methods are classified into two categories: dynamic simulation and static analysis. Dynamic simulation can reproduce or predict the time response of the system voltage to a sequence of events and, therefore, help identify whether the system voltage is stable or not. It is a valuable method to reveal the mechanisms of voltage instability and to verify the corrective strategies designed to improve voltage stability. However, the dynamic simulation method depends on proper modeling of numerous devices playing roles in the voltage instability and requires significant computation time for power systems with a reasonable size. Although the Quasi-Steady State (QSS) modeling technique, combined with the new class of computer simulation software can considerably reduce the simulation time, the dynamic simulation method is still too time consuming to be applied in real time. The majority of static methods are based on power flow formations to evaluate voltage stability in various terms, such as load margins, Jacobian matrix eigenvalues, and load flow feasibility. Various voltage stability indices (VSIs) based on these static analysis results have been proposed to indicate the distance between the current power system status to the voltage marginally stable point. These indices can be used to initiate different automatic voltage collapse countermeasures such as power system redispatch, var compensation device switching and load shedding. However these existing power flow based indices may be too slow to detect the short-term voltage instability as most power flow algorithms

depend on the power system state estimator, which is a part of the Supervisory Control and Data Acquisition (SCADA) and Energy Management System (EMS), to obtain the power system topology and other system variables. Even with modern high performance computer technology, the state estimation function typically takes minutes to update the snapshot of a power system. In addition, power flow algorithms normally do not consider load recovery dynamics, which is an important factor contributing to the voltage instability.

Technology advancements in the development of Intelligent Electronic Devices (IEDs) that are used for monitoring, protection, and control of power system operation have provided us new opportunities in the development of a new strategy for improving power system stability. Synchronized phasor measurement technology, which directly measures power system state variables (voltage phasors) and other variables, together with high-speed reliable communication infrastructures make it possible to build wide area measurement and protection systems [5] to complement classic protection and SCADA/EMS applications and to prevent cascading system level outages. The synchronized phasor measurement units (PMUs) have been recently available at a small cost as part of other substation measurements, for example, from protective relays [6]. These wide area measurement systems create new platforms for advanced high-speed wide area protection and control functions including voltage collapse prevention.

1.2 Objectives of the dissertation

The objective of this research is to develop a computationally efficient and reliable voltage stability index (VSI) based on synchronized phasor measurement

technology. The developed VSI is a reliable assessment of the voltage stability margin of an individual load and is suitable for on-line implementation for detecting the emerging short-term and long-term voltage instability. The sub-tasks of developing this improved voltage stability index are the following:

- Development of a new computationally efficient load margin assessment method based on synchronized phasor measurements and the power system network topology and parameters.
- Derivation of VSI of individual load buses and the power system based upon the calculated load margin.
- Implementation and testing of the new VSI on various power systems.

1.3 Outline of the dissertation

The dissertation is organized as follows:

Chapter 2 serves as an introduction to voltage stability problem. First, voltage stability is defined and classified, followed by an illustration of the voltage instability mechanism.

Chapter 3 reviews existing voltage stability assessment methods and briefly introduces existing voltage stability indices.

In Chapter 4, the limitations of existing VSIs are summarized and the need for an improved VSI is consequently justified. A work plan for developing a new VSI is presented as well.

Chapter 5 describes the development of the new voltage stability index. Starting with a simple two-bus power system model, a new load margin assessment method and

its related VSI are derived. Then the developed VSI is extended to load buses of a large, complex power system by simplifying the network behind each load bus into an equivalent single source and a single line model.

Chapter 6 shows the application of the proposed VSI on three widely used test systems. Test results are analyzed and discussed to verify the correctness and applicability of the proposed VSI. The summary and the future work are presented in Chapter 7.

CHAPTER II

VOLTAGE STABILITY PROBLEM

2.1 Introduction

Modern power systems are high-order, multivariable, dynamic systems whose responses to disturbances depend on the different characteristics of a wide array of devices. Power system stability generally refers to the capability of a power system to remain in a state of operation equilibrium under normal operation conditions and to regain an acceptable state of equilibrium after being subjected to disturbances [4,7]. Figure 2.1 shows the overall picture of the power system stability problem, which is categorized by the type of system variables in which instability can be observed and further by the time span that must be taken into consideration in order to assess the stability.

The rotor angle stability problem involves the study of electromechanical oscillations inherent in power systems and the ability of a power system to remain in synchronism after being subjected to a disturbance. Depending on the nature and size of the disturbance, the rotor angle stability is usually further characterized into two categories: small-signal stability and transient stability. Small-signal stability refers to the ability of the power system to maintain generator synchronization under small

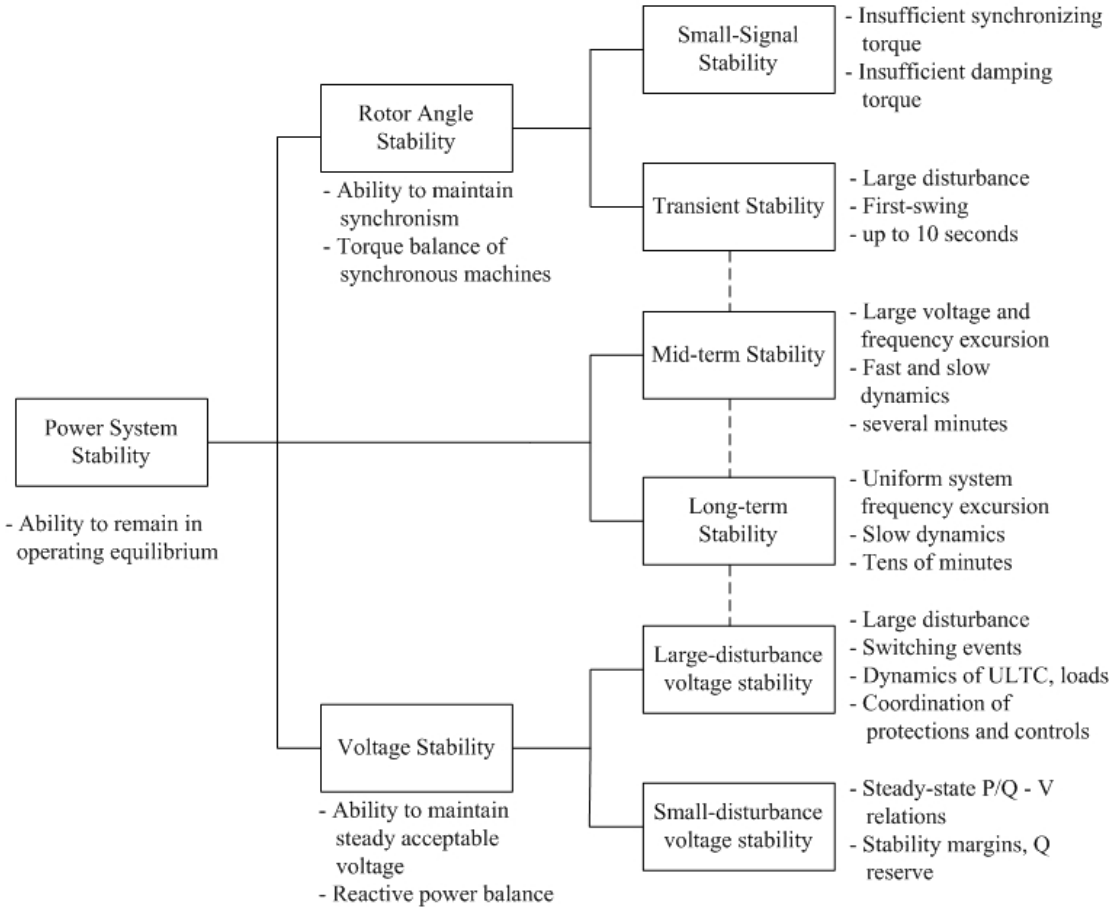

Figure 2.1 Classification of power system stability problems [4]

disturbances, such as small variations in loads and generation, while the transient stability refers to the ability of the power system to maintain synchronism after severe transient disturbances, such as a transmission line fault and tripping or loss of a generator unit [4]. Rotor angle stability has been the main focus of the system stability study by the power system community since the formation of the interconnected power system. As a result, it has been greatly mitigated by various technologies, such as fast operating circuit breakers, fast generator control systems, and various special power system stability controls. However, under stress conditions the power system may exhibit another type of unstable behavior, which is characterized by voltage drops at certain areas, escalating to cascading collapse without necessarily losing its synchronism between generators. This phenomenon is referred to as voltage collapse. Causes for voltage collapse include steady load increment and loss of transmission lines or generators. All the instability phenomena shown in Figure 2.1 may not be completely separated during power system collapse. Some power system blackout events have demonstrated that these instability phenomena happened at different stages as the system collapse evolves although causes of the blackouts are different. Historic analysis of power system blackouts reveals a general pattern:

- Most events happened when the power system had a heavy load.
- A series of initial outages of transmission lines or generators further weakened the power system.

- Partial power system oscillation started to happen, system frequency started to shift from the normal operation frequency, and the voltage started to deteriorate.
- More generators and transmission lines were tripped, and the system may split into small islands.

2.2 Definition and classification of voltage stability

2.2.1 Definition of voltage stability

As voltage instability involves a wide range of phenomena, voltage stability may mean different things to different engineers. A power system becomes voltage unstable when voltages uncontrollably decrease due to disturbances, such as an outage of equipment (generator, line, transformer, etc.), an increment of load demand, or a decrement in power generation. There are several definitions of voltage stability existing in the literature. These definitions consider time frames, system states, and large or small disturbances. The variations of the definition reflect the fact that there is a broad spectrum of phenomena that could occur during voltage instability.

1. *CIGRE Definition* [8]:
   - A power system at a given operating state is *small-disturbance voltage stable* if voltages near loads are identical or close to the pre-disturbance values following any small disturbance.

- A power system at a given operating state and subject to a given disturbance is *voltage stable* if voltage near loads approaching post-disturbance equilibrium value.
- A power system undergoes *voltage collapse* if the post-disturbance voltages are below acceptable limits.

2. *IEEE Definition* [9]:
   - *Voltage Stability* is the ability of a system to maintain voltage so that when load admittance is increased, load power will increase, and so that both power and voltage are controllable.
   - *Voltage Collapse* is the process by which voltage instability leads to loss of voltage in a significant part of the system.
   - *Voltage Security* is the ability of a system not only to operate stably, but also to remain stable (as far as the maintenance of system voltage is concerned) following any reasonably credible contingency or adverse system change.
   - A system enters a state of *voltage instability* when a disturbance, increase in load, or system change causes voltage to drop quickly or drift downward and operators and automatic system controls fail to halt the decay. The voltage decay may take just a few seconds or ten to twenty minutes. If the decay continues unabated, steady-state angular instability or *voltage collapse* will occur.

3. *IEEE/CIGRE Joint Definition* [7]:
    - *Voltage stability* refers to the ability of a power system to maintain steady voltages at all buses in the system after being subjected to a disturbance from a given initial operating condition.
    - *Voltage collapse* is the process by which the sequence of events accompanying voltage instability leads to a blackout or abnormally low voltage in a significant part of the power system.

The CIGRE definition is similar to other dynamic system stability problems. The IEEE definition emphasizes more the actual process of the power system network. The common ground between these definitions of voltage stability includes the following: voltage stability is a dynamic phenomenon, the system voltage must be controllable at the level that is acceptable, and the power system can survive disturbances to the system. Also, voltage collapse and voltage instability are interchangeable and both refer to the loss of voltage stability.

2.2.2 Classification of voltage stability

Power system stability is essentially the capability of the power system to maintain equilibrium with system variables in an acceptable range after being subjected to a wide range of disturbances no matter how small or large. The size of the disturbance influences the method of analysis and prediction of the stability. Voltage stability can be classified into the two following categories based on the size of disturbance [7,8]:

- *Large-disturbance voltage stability* refers to the ability of a power system to maintain steady acceptable voltages following a large disturbance, such

as system faults, loss of generation, or line tripping. The nonlinear response of a power system, including the interaction between numerous continuous and discrete control and protection devices, needs to be examined to determine large-disturbance voltage stability. Considering the nature of devices involved in a large system disturbance, the study period of interest may extend from a few seconds to tens of minutes.

- *Small-disturbance voltage stability* refers to the ability of a power system to maintain steady acceptable voltages when subjected to small perturbations, such as incremental changes of system load. For the analysis of small-disturbance voltage stability, it is reasonable to consider the linearized system model around the operation point. Discontinuous models for tap changing transformers and other equipment may be replaced with approximate continuous models. The study period of small-disturbance voltage stability may range from minutes to hours.

Figure 2.2 illustrates the time responses of different power system apparatuses to disturbances and voltage change. Considering the time range, voltage stability problems can be classified into two categories:

- Short-term voltage stability involves the dynamics of fast acting load components, such as induction motors, fast-controlled devices, and HVDC converters. The time frame of interest is several seconds, and analysis requires solution of appropriate system differential equations.

- Long-term voltage stability involves slower acting apparatuses, such as ULTC, thermostatically controlled loads, and overexcitation limiter (OXL). The time frame of interest ranges from several seconds to tens of minutes. Steady state or quasi-steady-state (QSS) analysis can be used to estimate stability margins, identify factors influencing stability, and devise remedial actions.

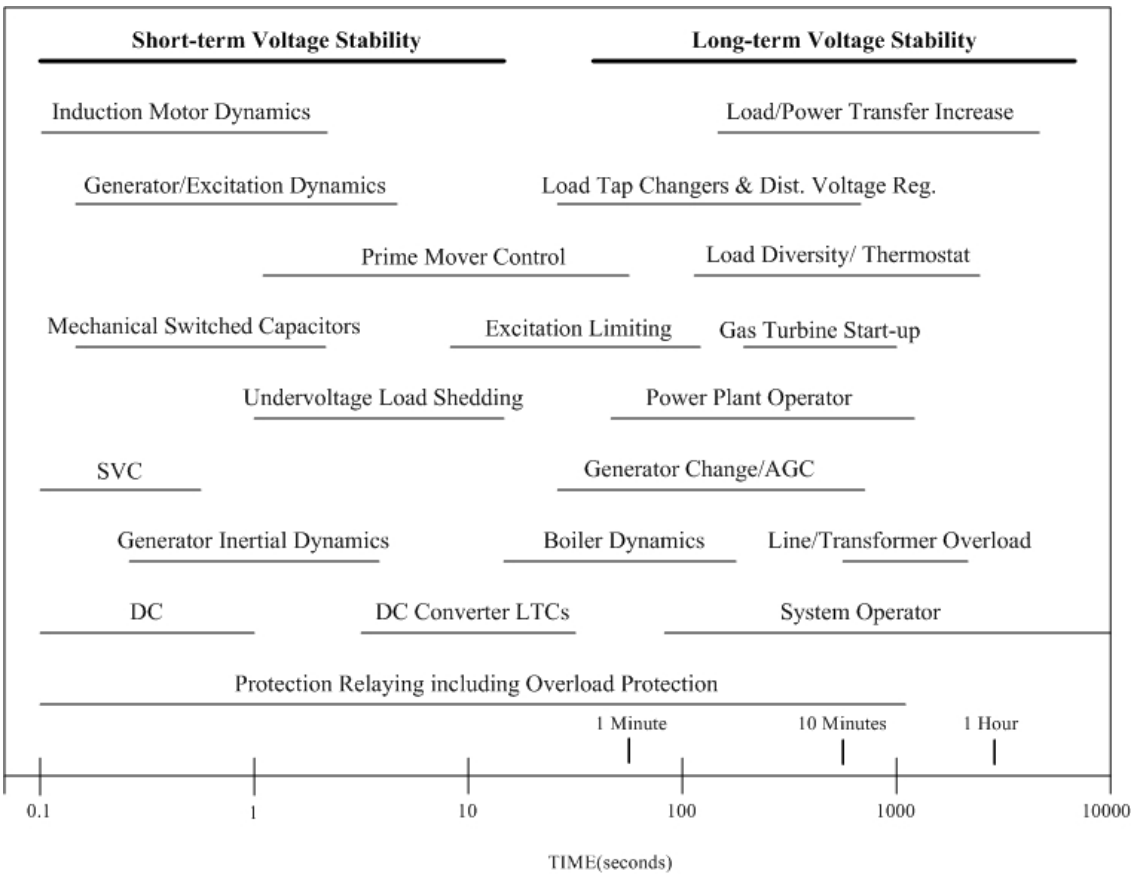

Figure 2.2 Time frame for voltage stability phenomena [2]

Proper classification of the voltage stability phenomena as shown above helps to reduce complex issues into a manageable problem by making simplifying assumptions. Different voltage stability problems can be analyzed using an appropriate degree of detail of system representation and appropriate analytical techniques.

2.3 Voltage collapse mechanism

Voltage stability is the capability of a power system to maintain the balance between load demand and the power that can be generated and transmitted to a load center. After a sudden voltage dip due to a disturbance, the aggregated load tends to restore its pre-disturbance power consumption through motor slip movement, a tap changing transformer, thermostats, and so on. When steady loads increase or the load restoration is beyond the capability of the transmission network and the power generation system, a run-down situation causing voltage instability occurs. Three important factors are involved in power system voltage instability: load demand, transmission network capacity, and power generation capacity. All three elements will be elaborated on individually as follows to show how they affect voltage stability.

2.3.1 Power system load

Load dynamic response to voltage variation is a key mechanism of power system voltage instability. Numerous technical papers have been written describing the nature of load and various approaches to modeling it. Activities are from different organizations, such as the IEEE task force and the CIGRE working group [10,11,12], and individuals [13,14]. The “load” can have different meanings to different power system engineers.

Depending on the type of analysis performed, the load models can be classified into two categories: static load models and dynamic load models.

A static load model characterizes the power consumed by the load as algebraic functions of the voltage magnitude. A widely used static load model is the exponential load model as shown by Equations 2.1 and 2.2, where P_o and Q_o are load consumptions at the reference voltage V_o and exponents α and β represent the load characteristics. Table 2.1 lists the exponents of some types of load. A special form of the exponential load model is the polynomial load model or ZIP load model, which consists of three types of load: constant impedance, constant current, and constant power. The real and reactive power consumption of the ZIP load model is shown by Equations 2.3 and 2.4, where $k_{Pz} + k_{Pi} + k_{Pp} = k_{Qz} + k_{Qi} + k_{Qq} = 1$. It is worth noting that these exponential load models are only valid when the load voltage magnitude is within a certain range (e.g. $0.6 < \frac{V}{V_o} < 1.2$). Outside this voltage range, the load characteristics may be completely different.

$$P(V) = P_o\left(\frac{V}{V_o}\right)^{\alpha} \tag{2.1}$$

$$Q(V) = Q_o\left(\frac{V}{V_o}\right)^{\beta} \tag{2.2}$$

$$P(V) = P_o\left[k_{Pz}\left(\frac{V}{V_o}\right)^2 + k_{Pi}\left(\frac{V}{V_o}\right) + k_{Pp}\right] \tag{2.3}$$

$$Q(V) = Q_o\left[k_{Qz}\left(\frac{V}{V_o}\right)^2 + k_{Qi}\left(\frac{V}{V_o}\right) + k_{Qq}\right] \tag{2.4}$$

Table 2.1 Exponents of different loads [3]

Load Type	α	β
Incandescent lamps	1.54	-
Air conditioners	0.50	2.5
Furnace fan	0.08	1.6
Battery charger	2.59	4.06
Electronic compact fluorescent	0.95-1.03	0.31-0.46
Conventional fluorescent	2.07	3.21

One definition of a load is the portion of the system that is not explicitly represented in the power system model, but rather is treated as if it were a single power-consuming device connected to a bus in the system model [11]. In this context, the aggregated load for transmission system analysis includes not only the connected power consumption devices, but also some of the following devices:

- Substation step-down transformers, including LTC
- Subtransmission and distribution feeders
- Voltage regulators
- Shunt capacitor banks and various reactive power compensation devices

The numerical representation of the aggregated load for voltage stability analysis involves several aspects that are not captured by static exponential load models. These factors include dynamics due to voltage sensitive loads, thermostatically controlled loads, voltage regulating device behavior, nonlinearities in voltage characteristics at low

voltages due to motor stalling and tripping, discharge lighting, and others. A good model of the aggregated dynamic load with these effects and reasonable computation efficiency is still the subject of ongoing investigation.

In references [13,14,15], simplified first order differential load models are proposed intending to capture the essential dynamic behavior of loads with different transient and steady state characteristics, such as thermostatically controlled loads and some motor-driven loads. While the form in which these models are presented appears quite different, they all, except [14], can be generalized to the block diagram shown in Figure 2.3, where X_p is an internal state variable modeling the load recovery dynamics and P_d is actual active power load. The active power load model is parameterized by steady state power P_s, transient power P_t , and load recovery time constant T_p. The P_s and P_t are expressed by Equations 2.5 and 2.6, where P_o is the rated power consumption of the aggregated load at the rated voltage V_o. Equations 2.7 and 2.8 represent the load model in a general dynamic system format. The only difference between [13] and [14] is that the summation between the transient power P_t and the internal state variable X_p is replaced by a multiplication.

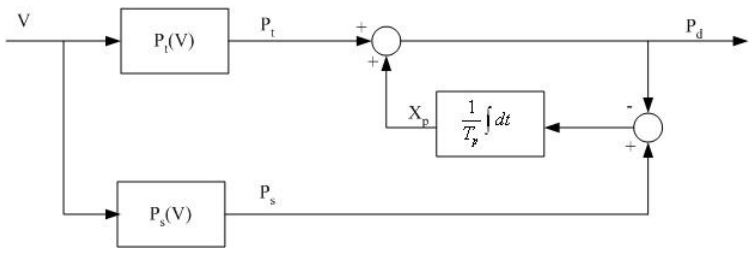

Figure 2.3 Simplified generic dynamic load model

$$P_t = P_o\left(\frac{V}{V_o}\right)^{\alpha_t} \tag{2.5}$$

$$P_s = P_o\left(\frac{V}{V_o}\right)^{\alpha_s} \tag{2.6}$$

$$\frac{dX_p}{dt} = \frac{1}{T_p}(P_s(V) - P_t(V) - X_p) \tag{2.7}$$

$$P_d = X_p + P_t(V) \tag{2.8}$$

A similar first-order differential system model is used for the load reactive power consumption, with corresponding characteristics $Q_t = Q_o\left(\frac{V}{V_o}\right)^{\beta_t}$, $Q_s = Q_o\left(\frac{V}{V_o}\right)^{\beta_s}$, and recovery time constant T_q. Typical values for these parameters are obtained through historical data analysis and are listed in Table 2.2. Figure 2.4 illustrates the load recovery dynamics in terms of voltage change, where T_p = 60 seconds, α_s = 1.5, and α_t = 2.0. Due to the load recovery dynamics, a power system, which survives a transient event, may experience potential long-term voltage instability as its loads tend to recover their power demand to the pre-disturbance level.

Table 2.2 Typical parameter values for generic load model [13]

T_p	T_q	α_s	α_t	β_s	β_t
60-300s	30-200s	0-2	1-3	2-5	4-6

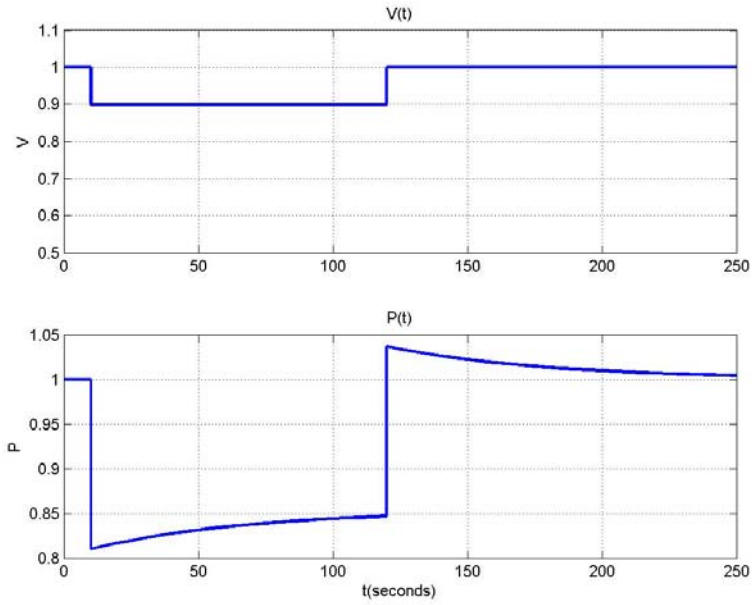

Figure 2.4 Load dynamics illustration

2.3.2 Line power transmission capacity

A major factor contributing to voltage instability is the voltage drop that occurs when active and reactive power flow through the line impedance of the transmission network. The transmission line impedances dictate the maximum power that can be transmitted through the lines between the source and the load. Under a deregulation environment, bulk power transfer over a long distance is primarily limited by the transmission system characteristics, as the transmission system was not originally designed for a large quantity of power transfer over long distances. Pushing the power transfer closer to the maximum capacity of the transmission network is one of the major causes of voltage instability.

To illustrate the maximum transferable power of the transmission lines, a simple two-bus power system model, as shown in Figure 2.5, is analyzed. The source with a

constant voltage, V_s, supplies a load through a transmission line, which is simplified to a reactance, jX. The active and reactive power received by the load can be expressed by Equations 2.9 and 2.10. Combining Equations 2.9 and 2.10 and eliminating the δ to solve the V_r, one can get Equation 2.11. Because V_r is a physical variable, a solution always exists. Therefore, the Inequality 2.12 should always be true.

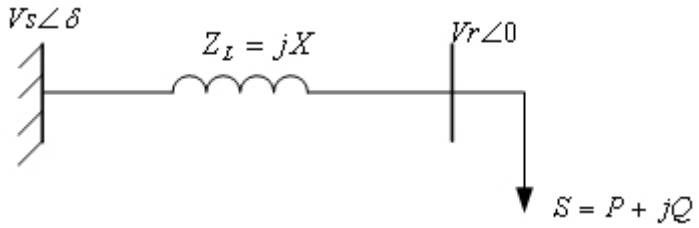

Figure 2.5 A two-bus power system model

$$P = \frac{V_s \cdot V_r}{X} \sin \delta \tag{2.9}$$

$$Q = \frac{V_s \cdot V_r}{X} \cos \delta - \frac{V_r^2}{X} \tag{2.10}$$

$$V_r = \sqrt{\frac{V_s^2}{2} - QX \pm X\sqrt{\frac{V_s^4}{4X^2} - P^2 - Q\frac{V_s^2}{X}}} \tag{2.11}$$

$$P^2 + Q\frac{V_s^2}{X} \le \frac{V_s^4}{4X^2} \tag{2.12}$$

As shown in Equation 2.11, the load voltage V_r depends on the sending end voltage V_s, line impedance X, and load demand values, P and Q. A three-dimensional surface, as shown in Figure 2.6, illustrates their relationship. Figure 2.7 is the same surface, but viewed from a side angle. The upper part of the surface corresponds to the higher voltage solution, which is the stable region. When the load voltage is at the lower

part of surface, which is the unstable region, an attempt to increase load demand further decreases the load voltage as explained by bifurcation theory [16]. Projecting the three-dimensional surface on the PQ plane produces a half-parabola as shown by Figure 2.8, which meets Inequality 2.12. The color part indicates the possible complex power, $S = P + jQ$, that can be transferred by this transmission line given a certain sending end voltage. The boundary of the color part indicates the complex power transfer limit, S_{max}, which is proportional to the square of the sending end voltage, V_s^2, and the line admittance, $\frac{1}{X}$. The maximum transferable active power, $P_{\max}$, is equal to $\frac{V_s^2}{2X}$ when $Q = 0$, while the maximum transferable reactive power, $Q_{\max}$, is equal to $\frac{V_s^2}{4X}$, which is half of the P_{max}, when $P = 0$. The maximum transferable active power decreases as the reactive power transfer increases. Similarly, the maximum transferable reactive power decreases as the active power transfer increases. Also, it is more costly to transfer the reactive power than the active power through the inductive line.

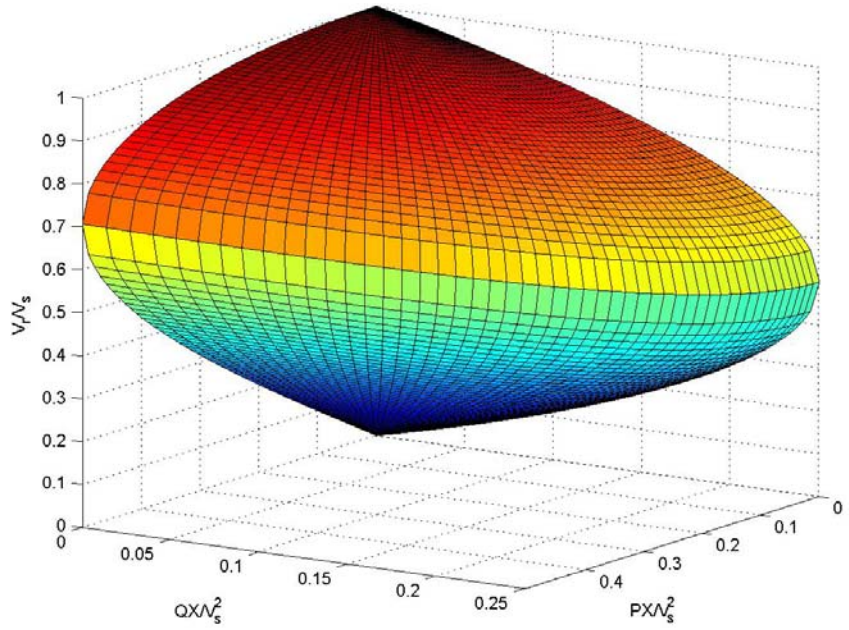

Figure 2.6 Three-dimensional plot of *PQV* (View from front)

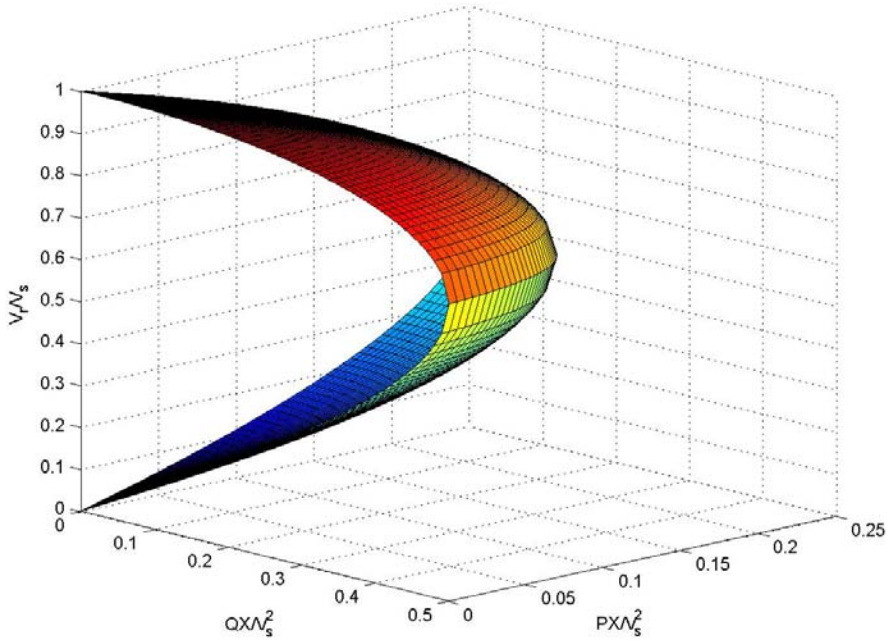

Figure 2.7 Three-dimensional plot of *PQV* (View from side)

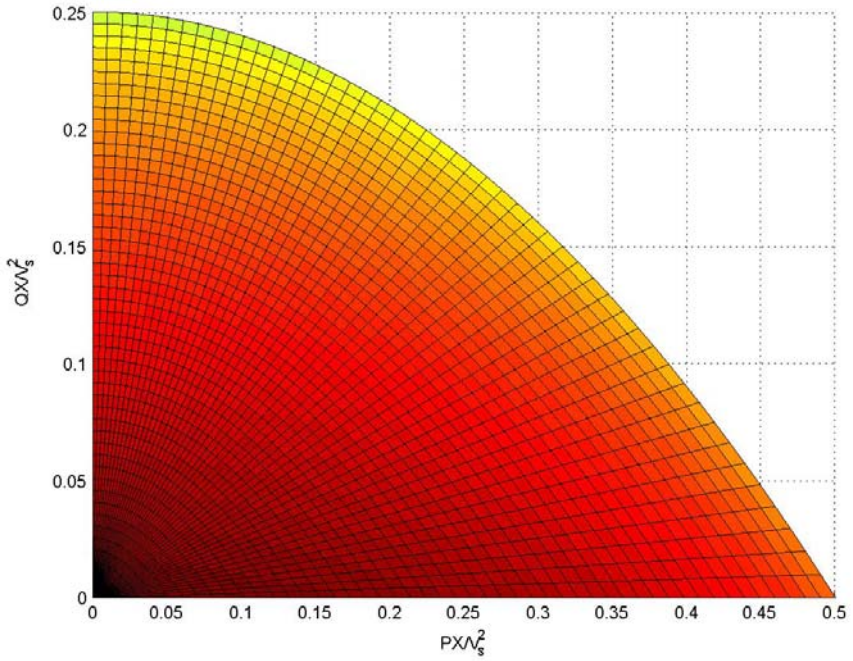

Figure 2.8 Transferable PQ power

2.3.3 Power generation capacity

Power generation capacity of the power system is of the same importance as the transmission system capacity to maintaining the system voltage stability. Normally, sufficient active power generation capacity is scheduled to supply the load and to withstand possible contingencies through proper power system operation planning. Reactive power generation, however, is more difficult to schedule, as the load reactive power demand normally increases as the system voltage decreases and it is more difficult to transfer reactive power through transmission lines. Under voltage stress conditions, induction motor loads are prone to stall and significantly increase the reactive power consumption. Contrary to this, the output of various reactive generation devices, such as the shunt capacitor bank, which are installed close to the load center, decreases as the

load voltage decreases. Therefore, the aggregated load reactive power demand increment due to load voltage decline increases the stress on the transmission networks and causes further voltage reduction. Voltage stability is threatened when a disturbance increases the reactive power demand beyond the sustainable capacity of the available reactive power resources. In almost all voltage instability incidents, at least one crucial generator is operating at its maximum reactive power generation capacity. As voltage stability is closely coupled with the system reactive power generation capacity, studying the characteristics and limitations of these reactive power generation equipment are of great importance for the analysis of the voltage stability problem.

Synchronous generators are the primary source of active and reactive power and to a great extent are responsible for the voltage support across the power system. The active power output of a generator is normally limited by the capacity of its primary mover. With the fixed active power output, the reactive power output is largely limited by its armature and field winding heat limits. When the power output is within the capacity limit of a generator, the terminal voltage of the generator is regulated by its automatic voltage regulator (AVR) and maintained constant. During conditions of system low voltages, the large reactive power demand may cause the field current and/or the armature current to reach its limit. Most modern generators have overexcitation limiters (OXLs) installed to prevent overheating on field circuits and rotors. Although there are some variations in the implementation of OXLs [17,18], the impacts of OXLs on general terminal voltage are similar. After the large generator output causes the excitation system field current to reach its limit, the generator field current is automatically fixed by its

OXL to the maximum permissible value. With the constant field current, the point of constant voltage is pulled back behind the synchronous reactance instead of at the generator terminal and, therefore, the generator loses its capability to maintain its terminal voltage constant. This mechanism equivalently increases the network reactance significantly [4]. Figure 2.9 illustrates the simplified steady-state equivalent circuit of a round-rotor synchronous generator, where V_t is the generator terminal voltage and X_s is the synchronous reactance. When the OXL reaches its limit, the i_{fd} and E_q are fixed instead of the V_t.

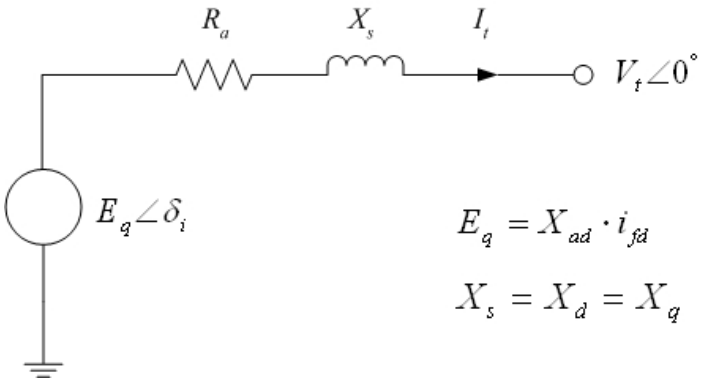

Figure 2.9 Steady-state equivalent circuit of a synchronous generator [4]

Equation 2.13 illustrates the relationship between the field current I_{fd} and the reactive power, Q, output of the round-rotor synchronous generator under steady-state condition as illustrated in Figure 2.9, where P is the active power output and X is machine internal impedance. The equation is in non-reciprocal per unit. When I_{fd} reaches the OXL limit due to the large reactive power demand, the machine terminal voltage V_t meets Equation 2.14, where the I_{fd_limit} typically ranges from 2.0 to 4.0 in per unit. Accordingly, the generator terminal voltage decreases as the reactive power out increases. From a

voltage support perspective, a constant generator terminal voltage indicates the generator still has a certain degree of reactive power generator capacity. Otherwise, an abnormally low generator terminal voltage indicates the generator has reached its capacity limit.

$$I_{fd}^2 = (V + X\frac{Q}{V})^2 + (X\frac{P}{V})^2 \tag{2.13}$$

$$V_{Q\_lim} = \frac{1}{2}\sqrt{2I_{fd\_limit} - 4X \cdot Q + 2\sqrt{I_{fd\_limit}^2 - 4X \cdot Q \cdot I_{fd\_limit} - 4X^2 \cdot P^2}} \tag{2.14}$$

There are three major types of reactive power compensation devices: shunt capacitors; SVCs; and series capacitors, used by utilities to provide reactive power and voltage support.

Shunt capacitors are the most inexpensive sources for providing reactive power and voltage support. They are typically installed close to the load center to reduce the need for long distance transmission of reactive power and save the controllable reactive power supply from generators and Static Var Compensators (SVCs). However, the reactive power generated by shunt capacitors is proportional to the square of the voltage. Under voltage stress conditions, the var support from the capacitor banks drops quadratically as the voltage drops, thus contributing to the voltage instability problem. In addition, voltage regulation becomes more difficult if the system is heavily compensated by shunt capacitor banks; stable operation is probably unattainable when shunt capacitor bank compensation is beyond a certain level [4].

SVC is a voltage controlled shunt compensation device that can either generate or absorb reactive power to regulate its bus voltage through automatically tuning its shunt susceptance. The typical operation speed of the SVC is within several cycles. Therefore,

SVCs are very effective in terms of mitigating angle instability and short-term voltage instability. There is no control or instability problem caused by an SVC within its regulating range. After reaching its limit, the SVC behaves as a mere shunt capacitor (or reactor), with the reactive power output proportional to the square of the voltage. A static var system (SVS) is an aggregation of SVCs and Mechanically Switched Capacitors (MSCs) or Reactors (MSRs) whose outputs are coordinated.

Series capacitors are occasionally installed on long transmission lines to reduce the line characteristic impedance and, therefore, increase the network transmission capacity. The reactive power supplied by series capacitors is proportional to the square of the line current and is independent of the bus voltages. It has a favorable affect on voltage stability. Because the series capacitors impose difficulties on the line protection systems and their maintenance is costly, series capacitor installation on the transmission system is limited, and its impact on the voltage stability is not very significant.

Voltage stability is directly related to the reactive power load-generation-transmission balance. Maintaining enough reactive power generation capacity is helpful for regulating system voltage and improving voltage stability. Rapid loss of reactive power generation reserve is a sign of impending voltage instability.

2.3.4 A simple example to illustrate the voltage instability

The simple power system shown in Figure 2.10 is used to illustrate the voltage instability mechanism. The source with a fixed voltage, $V_s\angle 0$, feeds the dynamic load through two parallel lines and an Under Load Tap Changing (ULTC) transformer. For the

sake of simplicity, the resistances of the two lines and the transformer are neglected and the load is assumed to be a purely active power load.

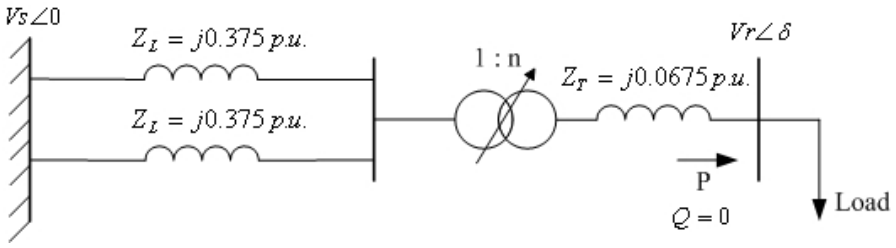

Figure 2.10 A three-bus power system to illustrate the voltage instability

The two dashed lines shown in Figure 2.11 illustrate the load steady state and transient characteristics, respectively. The rated load, P_0, is equal to 1.6 pu with transient exponential parameter, $\alpha_t = 2.0$, and steady exponential parameter, $\alpha_s = 1.2$. The outmost PV curve in black corresponds to the system with both transmission lines in service and ULTC ratio $n = 1.0$. Point A is the steady operational point during normal operating conditions. If one of the transmission lines is suddenly opened due to a fault clearance, the PV curve with a transformer tap position n equal to 1.0 shows the corresponding system PV curve before the tap-changer operates. Due to the sudden voltage change, the load demand complies with the load transient characteristics. Therefore, point B is the system operational point right after the line is opened. If the tap-changer is blocked after the line is opened, the system operational point will move from point B to point C along the PV curve with $n = 1.0$ as the load tries to restore the power from the transient to steady state condition. Because the operational point C is above the nose point, which corresponds to the maximum transferable power of the system, the

system operational point is finalized at the point C and the system voltage is stable. However, if the load voltage is below the minimum voltage threshold of the tap-changer after the line is opened, the ULTC automatically increases the transformer ratio n to restore the load voltage. As the ULTC finalizes its tap ratio at 1.1, which normally is the maximum tap ratio, the possible steady state operational point passes the nose point of the corresponding PV curve with n = 1.1. As the load tries to restore its demand, the system voltage decreases further along the lower part of the PV curve and the load voltage eventually collapses.

This simple power system is also modeled in Power Systems CAD (PSCAD) to obtain the time based dynamic simulation result. One of the transmission lines is opened at the 10th second. Figure 2.12 shows the load demand P (y axle) vs. time in seconds (x axle). Figure 2.13 shows the load voltage V_r (y axis) vs. time in seconds (x axis). Figure 2.14 shows the load voltage V_r (y axis) vs. load demand P (x axis), which matches the trajectory as shown in Figure 2.11.

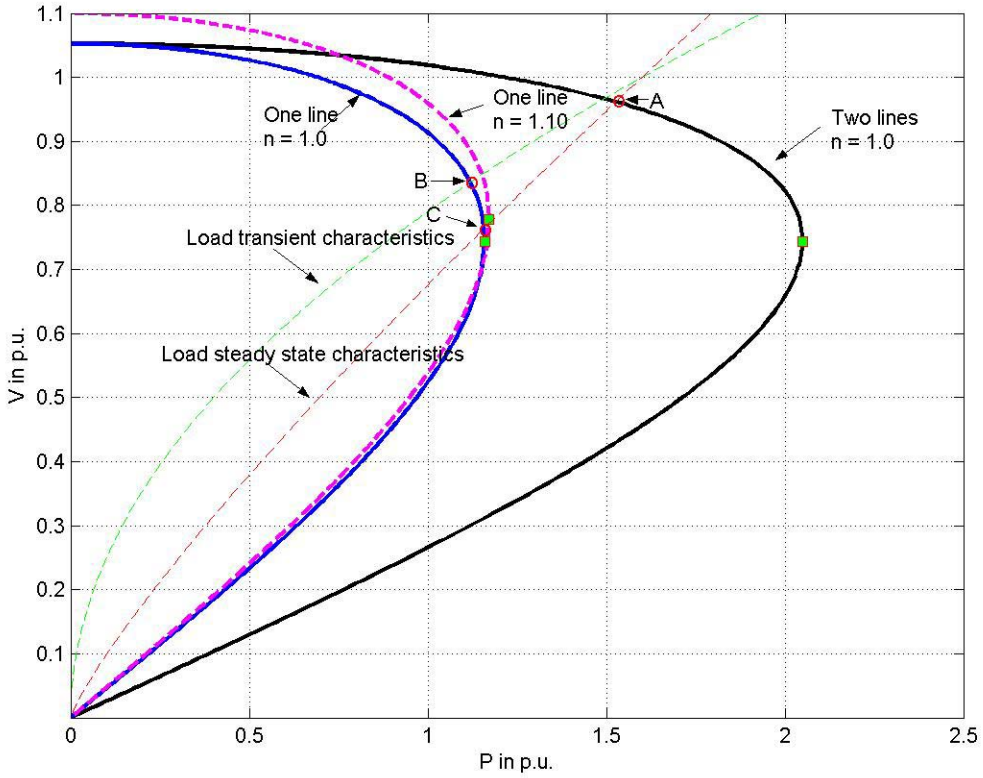

Figure 2.11 Steady state analysis results of the simple power system

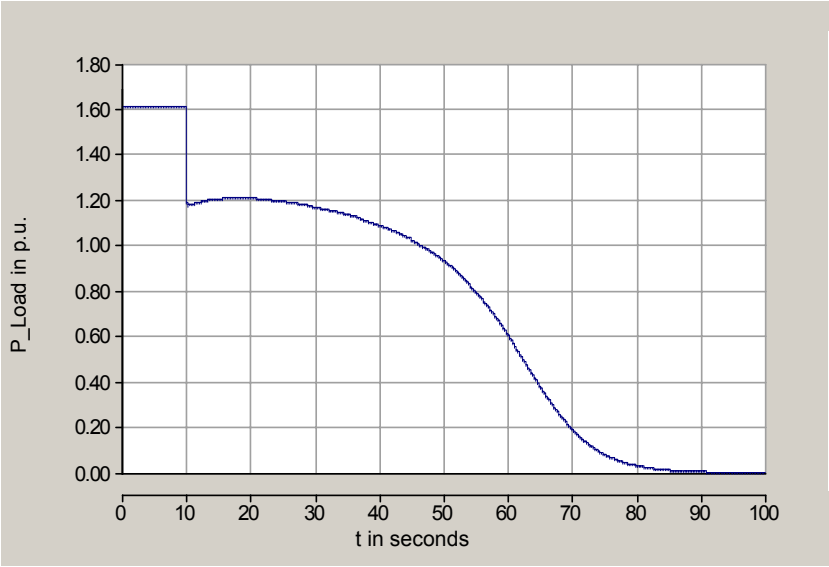

Figure 2.12 Load active power P versus time for Figure 2.10

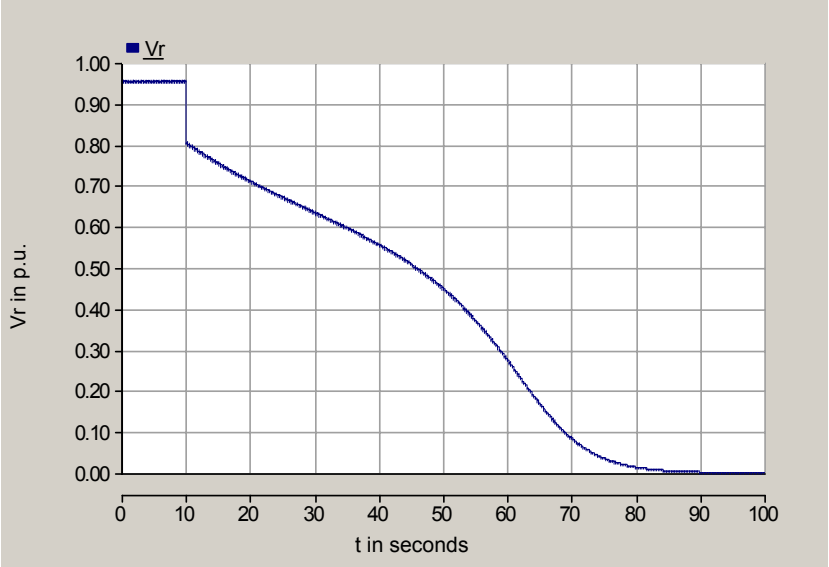

Figure 2.13 Load voltage V_r versus time for Figure 2.10

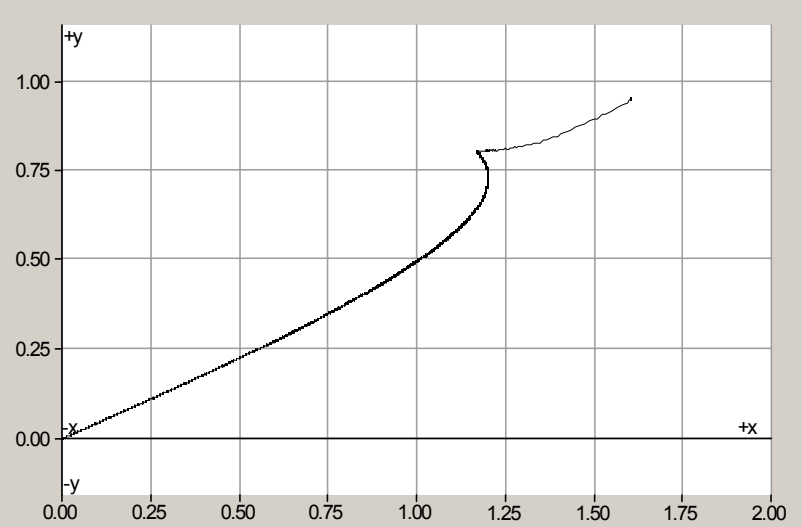

Figure 2.14 Load voltage V_r vs. load reactive power P for Figure 2.10

2.4 Summary

In this chapter, the definition and classification of the voltage stability problem are briefly introduced. Three important factors that affect the system voltage stability are summarized: load characteristics, line power transmission capacity, and power generation capacity of the system. One example is used to illustrate how the line transmission capacity and load dynamics together contribute to the voltage collapse. Voltage instability is a dynamic phenomenon. But, steady state analysis helps us to better understand the mechanism of voltage stability and, therefore, enables us to devise methods to mitigate the voltage instability problem.

CHAPTER III

LITERATURE REVIEW OF VOLTAGE STABILITY ASSESSMENT METHODS

Power systems are high-dimensional, nonlinear systems that operate in constantly changing environments; loads, generator outputs and key operating parameters are changing continuously. Therefore, voltage instability is a nonlinear, time variant, dynamic phenomenon. The existing voltage stability assessment methods and related VSIs can be classified into two categories: dynamic simulations and steady-state based analysis.

3.1 Power system dynamic modeling and simulation

A power system can be modeled by a large set of differential, discrete and algebraic equations as illustrated by Equations 3.1 - 3.4, where y represents the vector of bus voltages, x is the short-term state vector, and Z_c and Z_d are the continuous and discrete long-term state vectors, respectively[3]. Equation 3.1 captures the short-term system dynamics, such as generators, induction motors, HVDC components and SVCs. Equation 3.2 represents the power system long-term continuous dynamics, such as thermostatic load recovery and generator voltage regulator behavior. Equation 3.3 models the power system long-term discrete dynamics, such as LTC tap changes, shunt capacitor/reactor switching, and overexcitation limiters. The combination of Equations

3.2 and 3.3 models the power system long-term dynamics. Equation 3.4 stands for the equilibrium of the power system and is a set of network-based power flow equations.

$$\dot{x} = f(x, y, z_c, z_d) \tag{3.1}$$

$$\dot{z}_c = h_c(x, y, z_c, z_d) \tag{3.2}$$

$$z_d(k+1) = h_d(x, y, z_c, z_d(k)) \tag{3.3}$$

$$0 = g(x, y, z_c, z_d) \tag{3.4}$$

With reasonable simplifications and assumptions, a very detailed and fairly accurate model of a power system can be obtained based on the knowledge accumulated to date. A four-bus example system as shown in Figure 3.1 is modeled in detail by a set of equations as described in [3]. Tab. 3.1 lists the number of equations and variables. There are a total of twenty-two equations for modeling this four-bus system. This example illustrates that a large number of equations are necessary to model a realistic power system with hundreds or thousands of nodes. The Quasi Steady-State (QSS) approach [3,19] can reduce the number of the equations by assuming the power system is short-term stable and, therefore, replacing these short-term differential equations with fewer algebraic equations. Powerful simulation software packages equipped with advanced numerical solution methods, such as PSS/E and EUROSTAG, have been developed to handle the whole set of equations of large power systems and simulate system dynamics over a long period of time. Dynamic simulation can reproduce the time response of the power system to a sequence of events and help to identify whether the system is stable or not. However, time-domain simulations are still time consuming in

terms of computation burden and engineering work required for the modeling and analysis of results. Also, dynamic analysis does not provide much information regarding the sensitivity or stability margin. These issues prevent dynamic simulation from being used for on-line applications. Dynamic simulations are mostly used as tools for system planning, analysis, and protection and control system coordination studies.

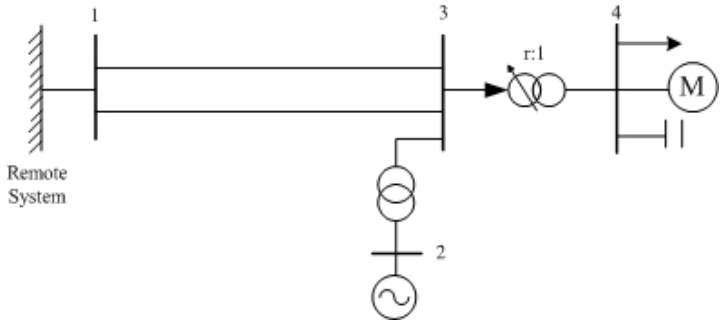

Figure 3.1 A four-bus power system [3]

Table 3.1 Dynamic model equations for the 4-bus example system [3]

3.1 Equations		3.1 Variables	
Short-term	8 equations	x :	Rotor angle δ, rotor speed ω, Internal voltage $E_q^{'}$, field voltage V_{fd}, Second exciter internal variable x_{oxl}, Induction machine slip S.
Long-term continuous	2 equations	z_c :	First exciter internal variable x_t
Long-term discrete	1 equation	z_d :	LTC tap position r
Network Equations	11 equations	y :	Bus voltage real part and imaginary part: v_{x1}, v_{y1}, v_{x2}, … v_{y4}

3.2 Steady-state analysis

As dynamic simulation for voltage stability analysis is unsuitable for on-line applications due to its high computation demand, significant research efforts have been devoted to finding various analytical techniques, including voltage stability indices (VSIs), to estimate the security of voltage stability based on the power system steady-state model. The steady–state model consists of only algebraic equations, such as the network Equation 3.4, and assumes all other time derivatives of the state variables (e.g. $\dot{x}$, $\dot{z}_c$) are equal to zero and discrete state variables are constant (e.g. $z_d(k+1) = z_d(k)$).

3.2.1 Power flow analysis

The steady-state power flow problem is directly derived from the network equations as shown in Equation 3.5, where I is the node injection current vector, Y is the network bus admittance matrix, V is the node voltage vector, and $S=P+jQ$ is the node injection complex power vector. Equation 3.5 can be further expanded to two nonlinear Equations 3.6 and 3.7, where P_i and Q_i are the active and reactive power injected at the bus, i, respectively; V_i and δ_i are the voltage magnitude and phase angle at bus i; and $Y_{ij}\angle\phi_{ij}$ is the ijth element of the complex bus admittance matrix Y.

$$Y \cdot V = I = \frac{S^*}{V^*} \tag{3.5}$$

$$P_i - V_i \sum_{j=1}^{N_{bus}} V_j Y_{ij} \cos(\delta_i - \delta_j - \phi_{ij}) = 0 \tag{3.6}$$

$$Q_i - V_i \sum_{j=1}^{N_{bus}} V_j Y_{ij} \sin(\delta_i - \delta_j - \phi_{ij}) = 0 \tag{3.7}$$

The underlying principle of the power flow problem is to solve for the bus voltages by solving the nonlinear equations given the system loads, generation, and network configuration. The most general and reliable algorithm to solve the power flow problem is the Newton-Raphson method [20,21], which involves an iterative solution of the linearized mismatch Equation 3.8 as the first term of a Taylor expansion of the nonlinear equations, Equations 3.6 and 3.7. The derivatives of the mismatch equations are summarized by Equations 3.9 - 3.16. The mismatch matrix is also called the Jacobian matrix.

$$\begin{bmatrix} \frac{\partial \Delta P}{\partial \delta} & \frac{\partial \Delta P}{\partial V} \\ \frac{\partial \Delta Q}{\partial \delta} & \frac{\partial \Delta Q}{\partial V} \end{bmatrix} \begin{bmatrix} \Delta \delta \\ \Delta V \end{bmatrix} = \begin{bmatrix} \Delta P \\ \Delta Q \end{bmatrix} \tag{3.8}$$

$$\frac{\partial \Delta P_i}{\partial \delta_i} = V_i \sum_{j=1}^{N_{bus}} V_j Y_{ij} \sin(\delta_i - \delta_j - \phi_{ij}) + V_i^2 Y_{ii} \sin \phi_{ii} \tag{3.9}$$

$$\frac{\partial \Delta P_i}{\partial \delta_j} = -V_i V_j Y_{ij} \sin(\delta_i - \delta_j - \phi_{ij}) \tag{3.10}$$

$$\frac{\partial \Delta P_i}{\partial V_i} = -\sum_{j=1}^{N_{bus}} V_j Y_{ij} \cos(\delta_i - \delta_j - \phi_{ij}) - V_i Y_{ii} \cos \phi_{ii} \tag{3.11}$$

$$\frac{\partial \Delta P_i}{\partial V_j} = -V_i Y_{ij} \cos(\delta_i - \delta_j - \phi_{ij}) \tag{3.12}$$

$$\frac{\partial \Delta Q_i}{\partial \delta_i} = -V_i \sum_{j=1}^{N_{bus}} V_j Y_{ij} \cos(\delta_i - \delta_j - \phi_{ij}) + V_i^2 Y_{ii} \cos \phi_{ii} \tag{3.13}$$

$$\frac{\partial \Delta Q_i}{\partial \delta_j} = V_i V_j Y_{ij} \cos(\delta_i - \delta_j - \phi_{ij}) \tag{3.14}$$

$$\frac{\partial \Delta Q_i}{\partial V_i} = -\sum_{j=1}^{N_{bus}} V_j Y_{ij} \sin(\delta_i - \delta_j - \phi_{ij}) + V_i Y_{ii} \sin \phi_{ii} \tag{3.15}$$

$$\frac{\partial \Delta Q_i}{\partial V_j} = -V_i Y_{ij} \sin(\delta_i - \delta_j - \phi_{ij}) \tag{3.16}$$

Nonlinear dynamic system analysis techniques, such as bifurcation theory, have been used to study voltage collapse and to devise ways of avoiding it. For some loads with special dynamic characteristics, the maximum loading point of the power generation and transmission system is not necessarily the saddle point node of the overall power system, and the system voltage may still be able to recover after the load demand passes the maximum loadable point [14]. But, for practical voltage stability analysis, the maximum loading point of the power system is often exchangeable with the voltage marginally stable point because chances are high that the system voltage will collapse if the load demand has reached the maximum loading point of the system and there is not any remedial action taken [16,22,23]. Therefore, almost all the power flow based voltage stability assessment methods and related VSIs are based on the approximation that the system load reaching the maximum loading point is equivalent to the system reaching the voltage marginally stable point.

3.2.2 PV/VQ curve and continuation power flow

System power flow analysis is often a useful tool for voltage stability analysis by monitoring system voltages as a function of load change. The maximum loading point of a particular load bus can be calculated by starting at the current operational point, making a small increment in load with an assumption of a certain load pattern (e.g. constant

power factor), and re-computing the power flow until the maximum loading point is reached. Meanwhile, P-V and V-Q curves for that load bus can be generated to visualize the maximum loading point. Figure 3.2 shows a set of PV curves with different load factors of the two-bus power system model as shown in Figure 2.5. For traditional power flow algorithms, the load point at which the power flow diverges and the Jacobian matrix of the system becomes singular is considered as the maximum loading point. A modification of the Newton-Raphson method known as the continuation power flow [24] method depends on a predictor-corrector scheme and introduces an additional equation so that the augmented Jacobian matrix is not singular at the maximum loading point. The continuation power flow method greatly facilitates the calculation of the maximum loading point and the plotting of complete PV and QV curves.

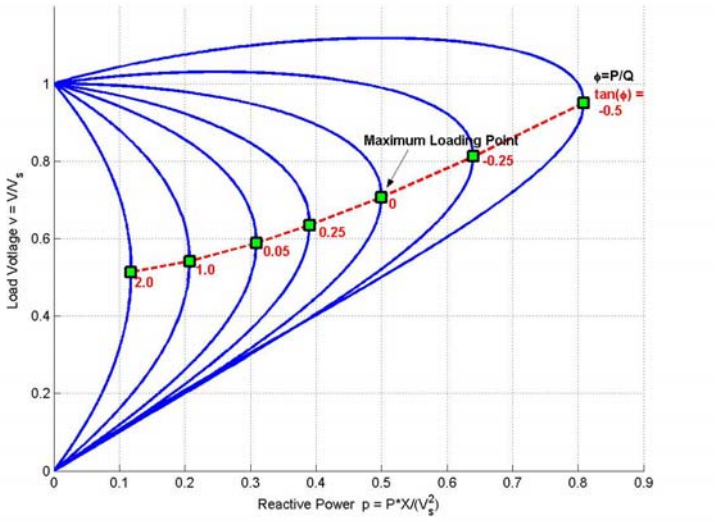

Figure 3.2 PV curves of the two-bus power system as shown in Figure 2.5

PV and QV curves are widely used by utilities for planning and analysis. But these curves are for individual load buses; that is, the stability characteristics are established by stressing each bus independently, which is not representative for realistic power system operation. Also, load increase patterns, which are normally hard to predict under voltage stress conditions, are normally assumed when calculating these curves.

3.3 Voltage stability indices

The main objective of VSIs is to estimate the distance from the current operating point to the system voltage marginally stable point. Numerical indices help operators to monitor how close the system is to collapse or to initiate automatic remedial action schemes to prevent voltage collapse. Most of the VSIs that have been proposed are based on steady state power flow formulations besides a couple of direct measurement based VSIs. The following important existing indices will be discussed:

- Singular values and eigenvalues of the power flow Jacobian matrix
- Sensitivity factors
- Existence of multiple power flow solutions
- Load flow feasibility
- Thevenin equivalent impedance
- Load margin
- Voltage
- Power system reactive power reserve

3.3.1 Singular values and eigenvalues of Jacobian matrix

When the power system steady-state load reaches the system maximum loading point, the corresponding Jacobian matrix of the power flow mismatch equation (Equation 3.8) becomes singular and, therefore, the conventional Newton-Raphson based power flow algorithms have difficulty with convergence. The full-sized Jacobian matrix can be further reduced to a matrix J_R, which presents only the linearized relationship between the change of bus voltage magnitude, ΔV, and bus reactive power injection, ΔQ, by making $\Delta P = 0$ as shown in Equation 3.17. Because the reactances of the transmission lines are much larger than their resistances, bus voltage magnitudes are more sensitive to ΔQ than ΔP. The reduced Jacobian matrix provides a convenient platform for system voltage stability evaluation as it focuses more on the study of the reactive power and voltage magnitude relationship and minimizes computational effort.

$$\Delta Q = \left[\frac{\partial Q}{\partial V} - \frac{\partial Q}{\partial \delta} \frac{\partial P}{\partial \delta}^{-1} \frac{\partial P}{\partial V} \right] \Delta V = J_R \Delta V \tag{3.17}$$

The minimum singular value and the minimum eigenvalue are two voltage stability indices that are obtained from the different decomposition methods of the same Jacobian matrix. And the interpretations of these two indices' results are also similar.

The singularity of a matrix is decided by the minimum singular value of the matrix, which can be obtained through singular value decomposition (SVD) as illustrated by Equation 3.18, where the u_i and v_i are the i^{th} columns of the orthogonal unit matrixes U and V respectively, and the matrix Σ is symmetrical with the diagonal values as σ_i and all other elements are zero.

$$J = U\Sigma V^T = \sum_{i=1}^{N} u_i \sigma_i v_i^T \tag{3.18}$$

The main diagonal values of matrix Σ are the singular values, which are nonnegative. If the minimum singular value is zero, the corresponding matrix is singular. Therefore the smallest singular value of the Jacobian matrix can be used as a secure index to determine how close the Jacobian matrix is to being singular and, consequently, how close the system is to being voltage instable. This method was first introduced by Thomas and Tiranuchi in [30,31]. To improve the computational speed of the SVD, Löf in [32] developed a fast algorithm to calculate the minimum singular value by preserving the sparsity of the Jacobian matrix.

The eigenvalue decomposition for the reduced Jacobian matrix, assuming it is diagonalizable, can be expressed by Equation 3.19, where Λ is a diagonal matrix of eigenvalues λ_i, Φ is the right eigenvector matrix of J_R, and Γ is the left eigenvector of J_R, and ϕ_i and γ_i are the i^{th} column of matrices Φ and Γ respectively. The eigenvalue λ_i is just a scalar that can vary from positive to negative.

$$J_R = \Phi\Lambda\Gamma = \sum_{i=1}^{N} \phi_i \lambda_i \gamma_i \tag{3.19}$$

Modal analysis of the power flow Jacobian matrix has revealed that if $\lambda_i > 0$, the i^{th} modal voltage and the i^{th} modal reactive power variation are along the same direction, indicating that the system is voltage stable. On the hand, if $\lambda_i < 0$, the i^{th} modal voltage and the i^{th} modal reactive power variation are along opposite directions, indicating that the system voltage is unstable. When $\lambda_i = 0$, the i^{th} modal voltage collapses because any

change in that modal reactive power causes infinite change in that modal voltage [25,26]. Under stable voltage conditions, all the eigenvalues are positive. The minimum eigenvalue moves towards zero and eventually becomes negative as the system transitions from a voltage stable condition to an unstable condition. Therefore the minimum eigenvalue can be used as a voltage stability index to detect voltage collapse.

Due to the quasi-symmetric structure of J_R, the eigenvalues and corresponding eigenvectors are expected to be real and very similar in value to the corresponding singular values and singular vectors. A study [27] has demonstrated that the minimum singular value and minimum eigenvalue basically provide similar information for static analysis of voltage collapse problems. These two indices are strongly non-linear to load change and do not provide much information about how close the system is to the marginally stable point nor of which buses are voltage critical until the system is very close to the marginal point. Although various improvements, such as the test function used in [28], have been proposed to reduce the computation costs, the matrix decomposition to calculate the minimum singular value and the minimum eigenvalue of the Jacobian matrix are still too computationally demanding for on-line applications.

3.3.2 Sensitivity factors

Sensitivity factors are reportedly used by utilities through the world as voltage stability indices to detect voltage instability because of their simplicity and computation efficiency [29]. Although eigenvalues and singular values are inadequate to detect proximity to static voltage collapse problems, they can provide theoretical proof of the

sensitivity factors. From Equations 3.17 and 3.18, we can get Equations 3.20 and 3.21, where ϕ_{rk} and γ_{rk} are the k[th] element of ϕ_r and γ_r respectively.

$$\frac{\Delta V}{\Delta Q} = \sum_{i=1}^{N} \frac{\phi_r \gamma_i}{\lambda_i} \tag{3.20}$$

$$\frac{\Delta V_k}{\Delta Q_k} = \sum_{i=1}^{N} \frac{\phi_{rk} \gamma_{ik}}{\lambda_i} \tag{3.21}$$

The V-Q sensitivity factor will change its sign, which indicates an "unstable" voltage condition, as the minimum eigenvalue gets closer to zero and changes its sign as well. It also can be observed from the PV and/or VQ curve of each load bus that the V-P and V-Q sensitivity increases along the upper part of the nose curves as load demand increases and theoretically reaches infinity at the nose point, which is the marginally stable point and is often referred to as the saddle-node bifurcation by static voltage analysis.

Q-V sensitivity factor based indices were proposed by [33,34]. Similarly, the ratio of the incremental change of reactive generation with respect to reactive demand and the change of system reactive power loss versus system voltage change were used as proximity indices to predict voltage instability in [29,35].

Sensitivity factor based indices are rather inexpensive to compute. This method can be implemented automatically in protection relays to initiate remedial actions, such as load shedding and capacitor bank switching, from the field to mitigate the voltage instability. However, these indices do not readily provide the distance to the marginally stable point and do not pinpoint the load areas that are more vulnerable to voltage collapse. Threshold settings for these indices-based remediation actions are difficult to

define. Operations of discrete control devices, such as LTC transformer and capacitor bank switching, can cause a discontinuity in these sensitivity indices and degrade their reliability.

3.3.3 Existence of multiple power flow solutions

There are two possible solutions to power flow equations under normal conditions, with one of these solutions corresponding to the true operational point of a power system. The number of existing solutions will change from 2 to 1 as the system operating point approaches the marginally stable point where only one solution exists. PV/QV curves can be used to illustrate this phenomenon, which is also confirmed in [36]. The authors in [36] further investigate the relationship between voltage instability and multiple load flow solutions by introducing a multilevel criterion, which consists of three criteria. A system is voltage stable if and only if all three criteria indicate voltage stability. Tamura et al. [37] used the pair of load flow solutions to calculate a voltage instability proximity index (VIPI).

The main obstacle of the multiple solution based voltage stability indices is the computation of the low voltage solution and avoidance of the power flow divergence at the marginally stable point. Even though various improved methods have been proposed to compute the low voltage solutions, difficulties still exist, particularly for lightly loaded systems. Also, the computational demand of these indices is too high for on-line applications.

3.3.4 Load flow feasibility

In [38], the authors propose a voltage stability index called the "L" indicator. The calculation of the "L" indicator is based on the general network equation as shown in Equation 3.22, where the buses are classified into two categories: generator bus and non-generator bus. Equation 3.22 can be reformulated into Equation 3.23, where sub-matrix F_{LG} is shown by Equation 3.24. An individual load bus "L" indicator is shown as Equation 3.25, where α_G is the number of generator buses, and system "L" indicator is shown as Equation 3.26 [38].

$$\begin{bmatrix} I_G \\ I_L \end{bmatrix} = \begin{bmatrix} Y_{GG} & Y_{GL} \\ Y_{LG} & Y_{LL} \end{bmatrix} \begin{bmatrix} V_G \\ V_L \end{bmatrix} \tag{3.22}$$

$$\begin{bmatrix} V_L \\ I_G \end{bmatrix} = \begin{bmatrix} Z_{LL} & F_{LG} \\ K_{GL} & Y_{GG} \end{bmatrix} \begin{bmatrix} I_L \\ V_G \end{bmatrix} \tag{3.23}$$

$$F_{LG} = -Y_{LL}^{-1} Y_{LG} \tag{3.24}$$

$$L_j = \left| 1 - \frac{\sum_{i=1}^{\alpha_G} F_{ji} \cdot V_i}{V_j} \right| \tag{3.25}$$

$$L_{sys} = \underset{\alpha_L}{MAX}\{L_j\} \tag{3.26}$$

The "L" indicator varies in the range between 0 (no-load of the system) and 1 (voltage collapse). A simplified "L" indicator by neglecting the real part of Y matrix is presented in [39] and applications of the "L" indicator for load shedding to prevent voltage collapse are presented as well.

The “L” indicator derivation is based on the feasibility of the power flow of the individual load bus. It has been shown that voltage collapse point of a two-bus system predicted by the indicator coincides with the point where the Jacobian matrix of the power flow is singular [39]. The advantage of the “L” indicator method is that the index can be calculated very easily and requires only the system Y matrix information and generator bus voltages. In addition, the load bus with the largest “L” indicator is identified as the load bus that is the most vulnerable to the voltage collapse corresponding to the maximum “L” indicator value. However, the “L” indicator output does not provide the distance to voltage collapse in a very “readable” format. As a result, the choice of threshold value of the indicator for initiating remedial actions is difficult to determine and is very subjective [39].

3.3.5 Thevenin equivalent impedance

Given a circuit as shown in Figure 3.3, circuit analysis shows that the load complex power is maximumized when $| Z_{load} | = | Z_{line} |$. The authors of [40,41] proposed a voltage stability index based on the ratio of the load equivalent impedance magnitude and the magnitude of the Thevenin equivalent impedance behind the load center. The voltage marginally stable point is declared when the ratio is equal to 1.

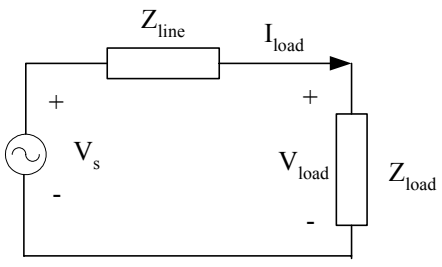

Figure 3.3 Thevenin equivalent circuit

The method appears to be appealing because of the simplicity and feasibility for implementation in local protection devices. Normally the load impedance Z_{load} can be easily calculated by dividing local measurements V_{load} with I_{load}. However, the remaining challenge is how to calculate accurately the V_{equ} and Z_{equ}, which includes the line impedance and source impedance, behind the load bus. Methods including the recursive least squares (RLS) algorithm have been proposed to calculate the Thevenin equivalent impedance [41], but still need to be improved in terms of accuracy and speed.

3.3.6 Load margin

Load margin is the most straightforward and widely accepted index of voltage collapse as it provides the amount of additional load that causes a voltage collapse. The load margin is obtainable through different methods, such as direct methods, continuation power flow methods, methods based on multiple power flow solutions and optimization methods. The method called the Point of Collapse (PoC) calculates the voltage collapse points (saddle-node bifurcations) directly as a solution of the non-linear equation (2.18) for which the Jacobian matrix is singular and its right or left eigenvector is a nonzero vector. The modified Newton-Raphson based power flow, called continuation power flow [42], as introduced previously, can also be used to calculate the maximum loading point. Authors of [43] propose a new method to calculate the load margin based on the information of the pair of power flow solutions. The load margin is defined as the point on the loadability boundary within the minimum Euclidean distance of the node injection changes. Optimization methods are also proposed to find the load margin by defining the

maximum load increment as the objective function and the power flow equations and generator reactive limits are equality and inequality restraints, respectively [44].

The high computation cost is the most serious disadvantage of the load margin method as illustrated by [45]. Also, the load margin calculation requires the assumption of a direction of load increase, which is often not readily available.

3.3.7 Voltage

Voltage is probably the simplest and most intuitive index for quantifying voltage stability. System voltage has been widely used by utilities as an index to initiate remedial actions such as undervoltage load shedding, to prevent voltage collapse. Various voltage-based load shedding schemes, including fixed time delay undervoltage and inverse time delay undervoltage load shedding, can be easily carried out by digital relays, which are broadly installed in the field without much additional cost [46,47]. Typically, voltage threshold is set between 85%-90% of the nominal voltage. The load to be curtailed is normally pre-selected as a fixed amount though simulations. Table 3.2 shows a three-stage undervoltage load shedding scheme that has been used by the affiliated utility of the authors of [46].

Table 3.2 Under-voltage load shedding scheme example [46]

	Voltage threshold (below lowest nominal voltage)	Time Delay	Amount of load to be shed
Stage 1	10%	3.5 seconds	5%
Stage 2	8%	5 seconds	5%
Stage 3	8%	8 seconds	5%

The limitation of the voltage based index is that it cannot quantify the distance to the voltage marginally stable point. As the PV curve with negative power factor shown in Figure 3.2 illustrates, a power system with heavy reactive power compensation may not demonstrate significant voltage depression even if the power transfer is close to the system transmission limit and the system is close to the voltage marginally stable point. In addition, the bus with the lowest voltage is not necessarily the one closest to the voltage collapse point. Therefore, pre-selected undervoltage based load shedding is not the optimal voltage instability mitigation scheme, as it has the risk of over load shedding.

3.3.8 Power system reactive power reserve

Power system voltage collapse is usually accompanied by some reactive power generation devices, such as generators and SVCs, reaching their capacity limits. High reactive power outputs and corresponding low reactive power reserve of the power system are sensitive indicators of voltage insecurity. On-line monitoring of reactive power consumption and reactive power reserves in the power system have been proposed as indices for voltage security assessment [48] and are being reportedly implemented at the BPA control center as described in [49,50]. Reactive power reserve is an intuitive index of the degree of system voltage security to system operators and can be used to identify the sub-region of the power system that is vulnerable for voltage collapse.

In [50], the author states that it is difficult to set the threshold for preventive countermeasures properly based on system level reactive power reserve because the required reactive power reserve of a particular group of generators and SVCs depends on

the possible contingencies and system operation conditions. In addition, the instability phenomena must to slow enough so that operator's action can be effective.

3.4 Summary

In this chapter, existing voltage stability assessment methods and some important VSIs are briefly summarized. Dynamic simulation of the power system responses to disturbances can reveal the voltage stability mechanism and demonstrate system stability with high confidence. However, the high computational demand of dynamic simulation based voltage stability assessment methods prohibits them from on-line applications. The majority of existing steady state voltage stability assessment methods and VSIs relate the voltage stability problem to the problem of solving the system power flow, which is a time-consuming, iterative process. These existing measurement based voltage stability indices, such as system voltage, are rough approximations of the voltage stability. They are unreliable to detect voltage marginally stable point and, therefore, may initiate remedial actions, such as load shedding, prematurely.

CHAPTER IV

STATEMENT OF PROBLEM AND WORK PLAN

4.1 Introduction

As power systems are high order non-linear systems, completely modeling the power system and using dynamic simulation to predict the system voltage stability are impractical for on-line applications given the size of a typical power system and the time range the voltage stability problem involves. Fortunately, the power system voltage stability problem is closely related to the balance between the load demand and the maximum loading point of the system. Hence, significant research effort aimed to mitigate the power system voltage stability problem has been devoted to finding reliable and computation efficient VSIs that can be used to initiate proper remedial actions to prevent voltage collapse. The existing VSIs can be broadly classified into two categories, namely power flow related indices and direct measurement based indices, as shown in Figure 4.1.

4.2 Limitation of existing indices

4.2.1 Power flow related indices

Power flow calculations are widely used by modern Energy Management Systems (EMS) application functions such as contingency analysis. State estimation functions

constitute the core of the EMS functions as it acts like a data filter between the raw measurements received from the Supervisory Control and Data Acquisition (SCADA)

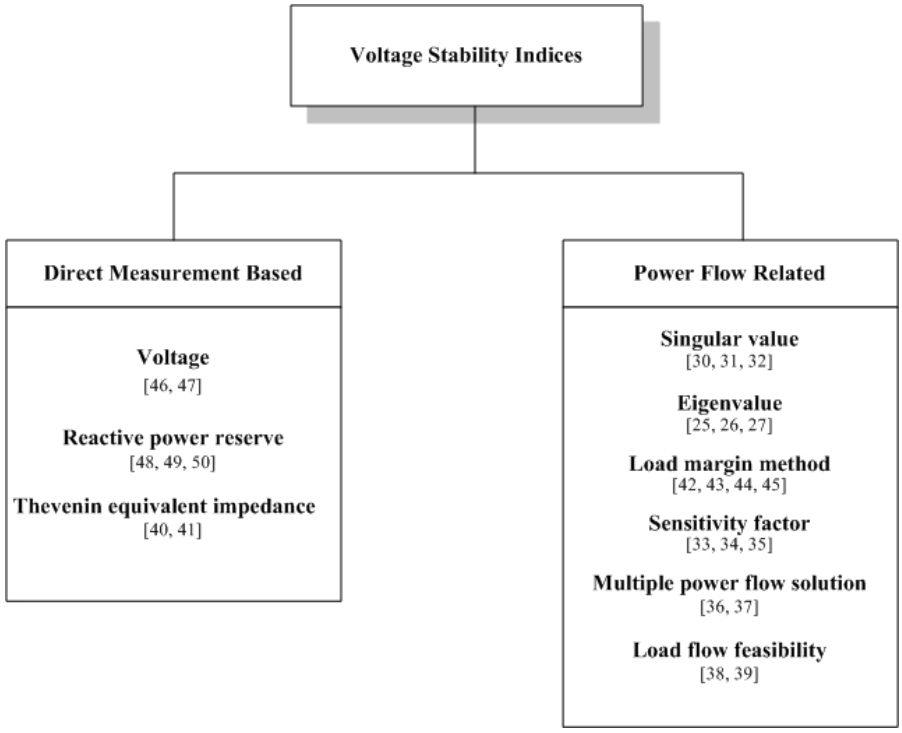

Figure 4.1 Voltage stability indices classification

system and all the application functions that require accurate data of the current state of the system. Traditional state estimation functions are based on iterative nonlinear estimation methods, such as the Weighted Least Squares (WLS) method, to obtain the system state variables, voltage phasors, and other system variables, such as load demands [51,52,53,54]. Because of the time skew in these measurement processes and the time (normally a few minutes) for estimation algorithms to converge, the analysis functions available from the EMS system have been largely restricted to steady-state phenomena. The limitation of these power flow based indices are summarized as follows:

- Conventional power flow based indices rely on a centralized EMS system, particularly the state estimator, which may be too slow to detect short-term and middle-term voltage instability phenomena.
- System modeling is largely limited to static models. Important factors, such as the generator field current limiter and the load dynamic reaction to low voltage, contributing to the voltage stability may not be sufficiently represented or may be neglected.
- Most of the power flow based indices proposed to date are computationally intensive, which is one of the major obstacles that prevents them from being used on-line.
- System operators, who mainly rely on EMS security analysis, may not have enough time to combat voltage instability effectively under stress conditions as too much information may be given by the EMS system.

4.2.2 Direct measurement based indices

Contrary to centralized EMS based voltage stability indices, direct measurement based VSIs can be implemented in protection devices to provide early detection of the voltage instability and prevent it from spreading system wide. The limitations of these existing direct measurement based VSIs are summarized as follows:

- Most direct measurement based VSIs do not accurately quantify the distance to the marginally stable point. Therefore, remedial actions, such as load shedding, initiated by these VSIs may be premature and may not meet the requirements of current utility practices.

- Threshold values for these VSIs are difficult to determine to initiate proper remedial actions. Numerous off-line simulations are normally required to determine the location of these measurements and the threshold values for these VSIs.

4.3 Synchronized phasor measurement

Recent successful commercialization of synchronized phasor measurement technology accompanied by high-speed communication networks has provided a new platform for developing new power system monitoring and control schemes. "Synchrophasor" or "synchronized phasor" refers to the phasor, a complex number in polar format, calculated from data samples using a standard time signal as the reference for the sampling process. With the standard time signal, the phasors from remote sites have a defined common phasor relationship [55]. The device that provides synchronized phasor measurement is usually called a Phasor Measurement Unit (PMU). A PMU is not necessarily a special device. Now, more and more digital relays also provide synchronized phasor measurements, especially in transmission or sub-transmission networks. Figure 4.2 illustrates a general structure of a PMU. The common time source for synchronization is from a Global Positioning System (GPS) receiver, which can decode time synchronized to within 0.2 μs of Greenwich Mean Time (GMT), the world time standard [55]. PMUs and high-speed communication networks compose the wide area measurement system that brings the direct measurements of power system state variables together almost in real time and are able to measure the dynamics of the power system. Several WAMSs are being installed on a trial basis throughout the world. Some

advanced wider area protection and control applications have been developed based on these WAMSs to improve the power system stability [5].

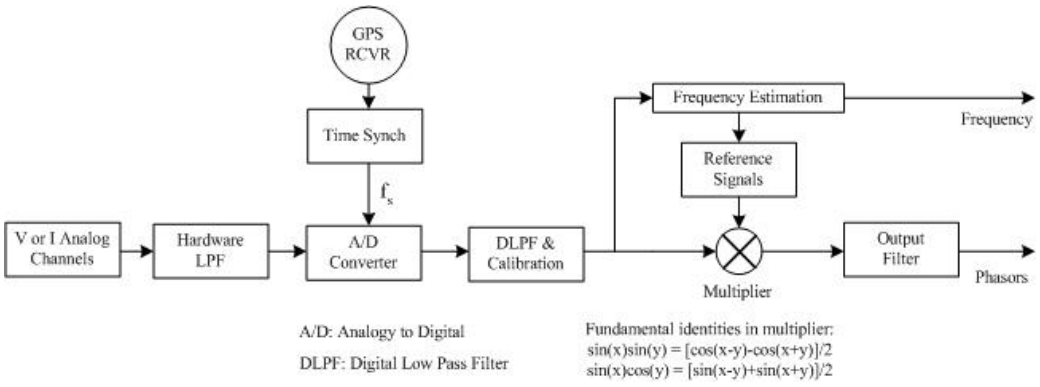

Figure 4.2 General structure of PMU [6]

4.4 Motivation

Power system voltage stability problems have been well recognized and much work has been done to date on the development of effective off-line voltage stability analysis methods and tools to mitigate the potential voltage instability at the stage of system design and operations planning. However, many utilities are still limited to performing off-line studies to determine the voltage stability margins and necessary control actions to maintain the stability of systems based on the analysis of only a small number of operational conditions and contingencies. These developed voltage stability analysis methods, based on the traditional EMS system, have an inherent limitation in speed and static modeling and, therefore, have not been reportedly used for any successful on-line application. On the other hand, applying automatic under-voltage load shedding to prevent voltage collapse is being adopted by more utilities today, as it can be

easily implemented through digital relays and the decision is made based on the local information. A reliable and optimal VSI, other than voltage, suitable for on-line application is of great value and is still attracting great interest from the power engineering community. Since these synchronized phasor measurements are available, this research work is directed towards developing an improved on-line VSI that not only can reliably detect the system marginally stable point but also is computationally efficient for on-line applications.

4.5 Work plan

In order to reduce the voltage stability assessment problem to a manageable issue, this work narrowly focuses on the root cause of the voltage instability. That is, voltage collapse starts when the load power demands surpass the maximum power that can be generated and transferred to the load center. Voltage instability could also originate as a local phenomenon and then become a system level problem if countermeasures are not taken early enough to contain the problem in that area. This research starts with a derivation of the maximum transferable power of a simple power system. The fact that the maximum transferable active power and reactive power are mutually exclusive and that the load factor affects the maximum transferable power will be taken into consideration. Once the maximum transferable power is obtained, a VSI has been devised based on the load margin that is the difference between the maximum transferable power and the load power consumption measurement. To apply the VSI on a large power system, the large complex network behind a load bus will be first simplified into a single source and single line model. The simplified model should preserve the power flow

results and voltages of the load bus, as the power balance is a key issue of analysis for voltage stability. Then the VSI of each load bus can be calculated based on the corresponding simplified single source system model. The VSI of the load bus that has the minimum load margin will be chosen as the VSI of the system. Three common test cases will be used to validate the devised VSI.

The next chapter provides details on the derivation of the VSI. Chapter VI includes validation of the VSI with the BPA 10-bus, IEEE 30-bus, and CIGRE 32-bus test cases.

CHAPTER V

IMPROVED VOLTAGE STABILITY INDEX DEVELOPMENT

5.1 Introduction

The voltage stability problem normally starts as a local phenomenon and then becomes a system level problem if no countermeasures are taken. Preventing the system voltage at every load center from passing the marginally stable point is an effective and economical measure to prevent voltage collapse. As shown in Chapter 2, the power system voltage stability problem is tightly coupled with the power system load demand problem. More specifically the power system voltage marginally stable point, in most cases, coincides with the maximum deliverable power by the generation and transmission system. To most utilities today, the maximum deliverable power is often limited by the maximum transferable power capacity of the transmission networks, especially under contingency situations. Hence, obtaining the maximum deliverable power to each load center is equal to finding the voltage marginally stable point.

The derivation of the improved VSI starts with a simple system model and then is extended to a generic large power system model. Finally, some practical issues related to the implementation of the VSI are discussed.

5.2 Voltage stability index for simple power system

5.2.1 Maximum transferable power through a transmission line

Given a simplified power system model as shown in Figure 5.1, the source with voltage magnitude V_s supplies a remote load through one transmission line with line impedance as $Z = R + jX$. Knowing the receiver voltage magnitude, V_r, and the phasor angle difference, δ, between the source voltage and load voltage, the complex power, S, received at the load end can be expressed by Equation 5.1. Equations 5.2 and 5.3 show the active power P and reactive power Q, respectively. Combining Equations 5.2 and 5.3 by eliminating δ and rearranging the results, we can get a second-order equation with respect to the receiver voltage magnitude, V_r^2, as shown by Equation 5.4. Equation 5.5 expresses the numerical solution of the V_r, which is a function of V_s, P, Q, R and X. As the receiver voltage magnitude, V_r, is a physical quantity, there must always be a solution. That means the part under the second square root in the Equation 5.5 should not be less than zero, as shown by Inequality 5.6.

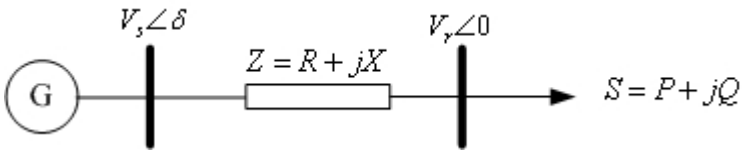

Figure 5.1 Single line power system model

$$P + jQ = V_r \cdot \left(\frac{V_s\angle\delta - V_r}{R + jX} \right)^* \tag{5.1}$$

$$P = \left[(V_s \cdot \cos(\delta) - V_r) \cdot \frac{R}{R^2 + X^2} + V_s \cdot \sin(\delta) \cdot \frac{X}{R^2 + X^2} \right] \cdot V_r \tag{5.2}$$

$$Q = \left[(V_s \cdot \cos(\delta) - V_r) \frac{X}{R^2 + X^2} - V_s \cdot \sin(\delta) \cdot \frac{R}{R^2 + X^2} \right] \cdot V_r \tag{5.3}$$

$$V_r^4 + \left(2X \cdot Q + 2P \cdot R - V_s^2\right) \cdot V_r^2 + \left(P^2 + Q^2\right) \cdot \left(R^2 + X^2\right) = 0 \tag{5.4}$$

$$V_r = \sqrt{\frac{V_s^2}{2} - (X \cdot Q + P \cdot R) \pm \sqrt{\frac{V_s^4}{4} - (Q \cdot X + P \cdot R) \cdot V_S^2 - (P \cdot X - Q \cdot R)^2}} \tag{5.5}$$

$$\frac{V_s^4}{4} - (Q \cdot X + P \cdot R) \cdot V_S^2 - (P \cdot X - Q \cdot R)^2 \geq 0 \tag{5.6}$$

When the left part of the Inequality 5.6 equals zero, there is only one possible solution of V_s and the system voltage is at the marginally stable point, as the load demand has reached the maximum transferable complex power, S_{max}, through this transmission line given the source voltage magnitude V_s. Further attempts to increase the load demand draws the receiver voltage V_r from the high value to the low value as the voltage starts to collapse. From Inequality 5.6, the range of P and Q with respect to each other can be obtained as shown by Inequalities 5.7 and 5.8, where $|Z| = \sqrt{R^2 + X^2}$. Since we are interested in the power flow direction from the source to the load, the maximum transferable active power P_{max} through that line can be expressed by Equation 5.9. Similarly, the maximum transferable reactive power Q_{max} is expressed by Equation 5.10. If the load is maintained as a constant power factor with the power angle $\theta = atan(\frac{Q}{P})$, the maximum transferable complex power S_{max} can be expressed by Equation 5.11. For

transmission lines with a high ratio of X/R, the approximate P_{max}, Q_{max} and S_{max} can be expressed in Equations 5.12 – 5.14 by neglecting the line resistance R.

$$\frac{Q\cdot R}{X}-\frac{V_s^2\cdot R}{2X^2}-\frac{|Z|\cdot V_s\cdot\sqrt{V_s^2-4Q\cdot X}}{2X^2}\le P\le\frac{Q\cdot R}{X}-\frac{V_s^2\cdot R}{2X^2}+\frac{|Z|\cdot V_s\cdot\sqrt{V_s^2-4Q\cdot X}}{2X^2} \tag{5.7}$$

$$\frac{P\cdot X}{R}-\frac{V_s^2\cdot X}{2R}-\frac{|Z|\cdot V_s\sqrt{V_s^2-4P\cdot R}}{2R^2}\le Q\le\frac{P\cdot X}{R}-\frac{V_s^2\cdot X}{2R}+\frac{|Z|\cdot V_s\sqrt{V_s^2-4P\cdot R}}{2R^2} \tag{5.8}$$

$$P_{max}=\frac{Q\cdot R}{X}-\frac{V_s^2\cdot R}{2X^2}+\frac{|Z|\cdot V_s\cdot\sqrt{V_s^2-4Q\cdot X}}{2X^2} \tag{5.9}$$

$$Q_{max}=\frac{P\cdot X}{R}-\frac{V_s^2\cdot X}{2R^2}+\frac{|Z|\cdot V_s\sqrt{V_s^2-4P\cdot R}}{2R^2} \tag{5.10}$$

$$S_{max}=\frac{V_s^2\cdot\left[|Z|-(\sin(\theta)\cdot X+\cos(\theta)\cdot R)\right]}{2(\cos(\theta)\cdot X-\sin(\theta)\cdot R)^2} \tag{5.11}$$

$$P_{max}=\sqrt{\frac{V_s^4}{4X^2}-Q\frac{V_s^2}{X}} \tag{5.12}$$

$$Q_{max}=\frac{V_s^2}{4X}-\frac{P^2\cdot X}{V_s^2} \tag{5.13}$$

$$S_{max}=\frac{(1-\sin(\theta))\cdot V_s^2}{2\cos(\theta)^2\cdot X} \tag{5.14}$$

We observe from Equations 5.9 – 5.14 that P_{max} and Q_{max} increase as the source voltage magnitude, V_s, increases or the line impedance, Z, decreases. Also P_{max} decreases as Q increases, as illustrated by Figure 5.2. Similarly, Q_{max} decreases as P increases, as illustrated in Figure 5.3. Figure 5.4 illustrates that the maximum transferable complex power, S_{max}, increase as the power factor, $\alpha=\cos(\theta)$, increases.

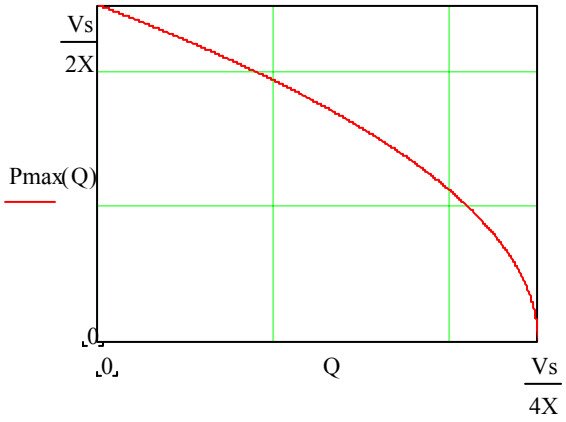

Figure 5.2 Maximum transferable active power P_{max} vs. reactive power Q

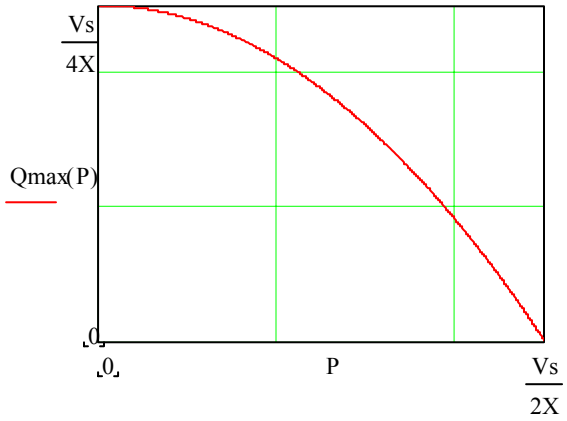

Figure 5.3 Maximum transferable reactive power Q_{max} vs. active power P

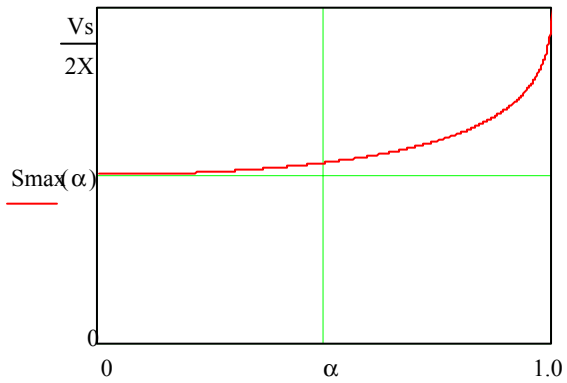

Figure 5.4 Maximum transferable complex power S_{max} vs. load power factor α

5.2.2 *Load margins of the single line system*

Load margin refers to the amount of additional load (complex power) demand that would cause the power system voltage to reach the marginally stable point, as the power system voltage stability problem stems from the load demand surpassing the maximum power that can be generated and transferred to the load center. The system voltage stability security is proportional to the load margin. A popular approach in the power industry to determine the steady state maximum load point is the repetitive power flow calculation by increasing load with respect to a given load increase pattern. The load that causes the power flow calculation not to converge is claimed to be the maximum load. As can be seen from Section 5.2.1, the maximum transferable complex power and, therefore, the load margin depend on the aggregated system load characteristics, such as the power factor, which are difficult to predict because of the dynamic nature of the aggregated system load reacting to a voltage variation. For example induction motors may stall at low voltage and draw significant reactive power as compared to their rated reactive power. Therefore the steady state calculated load margin is unsuitable of on-line applications, especially when the system voltage is abnormal. Alternatively, three load margins that are suitable for on-line applications are proposed here and shown by Equations 5.15 – 5.17, where P_{max}, Q_{max}, and S_{max} are shown in Equations 5.9 – 5.11. The P, Q, and S are the present power demand of the load. The calculated, P_{margin}, is based on the assumption that the reactive power demand, Q, is constant. Similarly the calculated Q_{margin} is based on the assumption that the active power demand, P, is constant. The calculated S_{margin} is based on the assumption that the present load power factor is

preserved as the load increases. An additional assumption is that the source voltage magnitude is maintained as a constant. The calculated P_{margin} and Q_{margin} are relatively overly optimistic because normally the active power and reactive power demand increase simultaneously. In spite of these assumptions, these three load margins predict the distance from the current load demand to the maximum load demand that may cause the voltage collapse in a meaningful and interpretable way. Also the three load margins will become zero simultaneously as the load demand reaches the maximum load demand and the system voltage approaches the marginally stable point. The proposed load margin calculation method can be applied to an individual load bus and its computation efficiency makes it suitable for on-line applications.

$$P_{margin} = P_{max} - P \tag{5.15}$$

$$Q_{margin} = Q_{max} - Q \tag{5.16}$$

$$S_{margin} = S_{max} - S \tag{5.17}$$

Example 5.1

Given the line parameter of the simplified power system model shown in Figure 5.1 $Z = 0.012 + j0.101\ pu$ and the $V_s = 1.0\ pu$, the load power factor, α, evenly decreases from 0.95 to 0.80 in 10 seconds together with the complex power, S, evenly increasing from 0 pu to the maximum transferable complex power, $S_{max} = 1.746\ pu$, corresponding to $\alpha = 0.8$.

Figures 5.5 –5.7 demonstrate that the calculated P_{max}, Q_{max} and S_{max} merge with the corresponding load demand P, Q and S simultaneously at the voltage marginally stable point as shown in Figure 5.8, in which the upper part (solid line) represents the real load voltage and the lower part (dashed line) represents the other possible voltage solution. Figure 5.9 shows the three load margins, which decrease as the load demand increases and become zero when the load demand reaches the maximum transferable load.

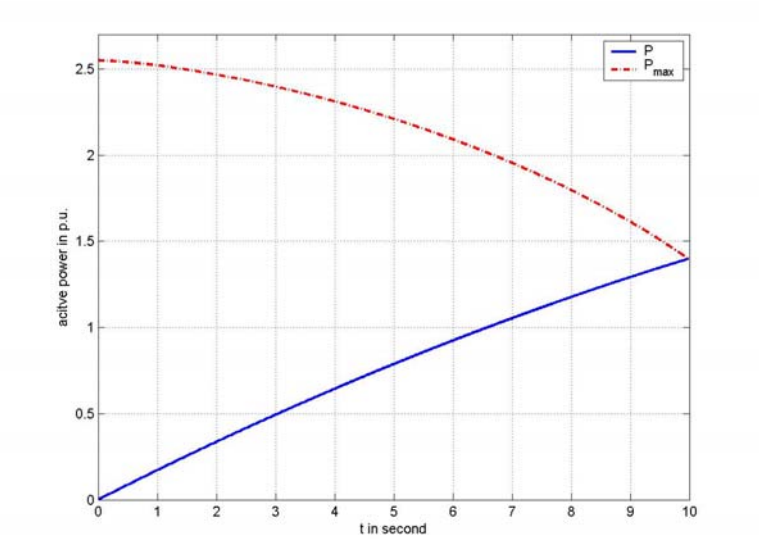

Figure 5.5 Predicted P_{max} vs. P for system in Example 5.1

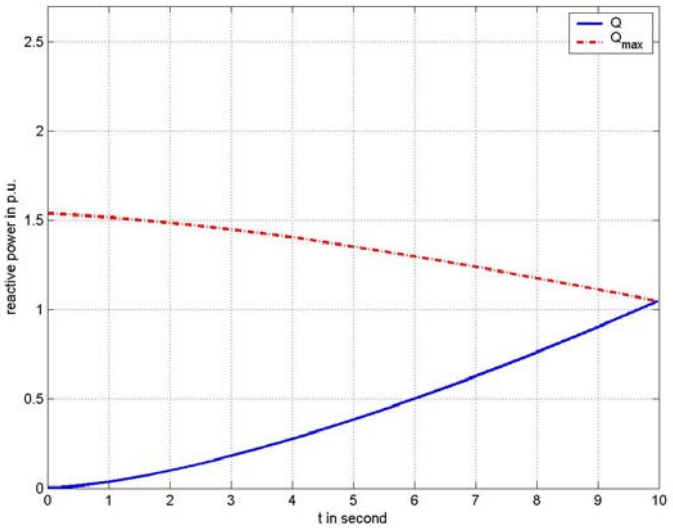

Figure 5.6 Predicted Q_{max} vs. Q for system in Example 5.1

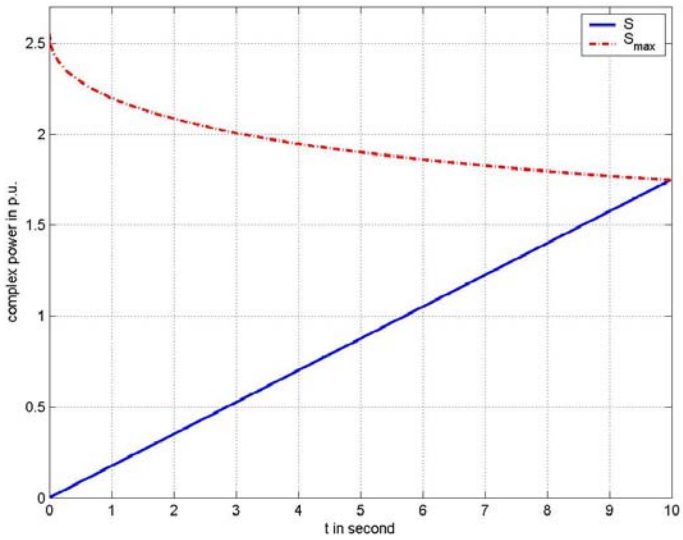

Figure 5.7 Predicted S_{max} vs. S for system in Example 5.1

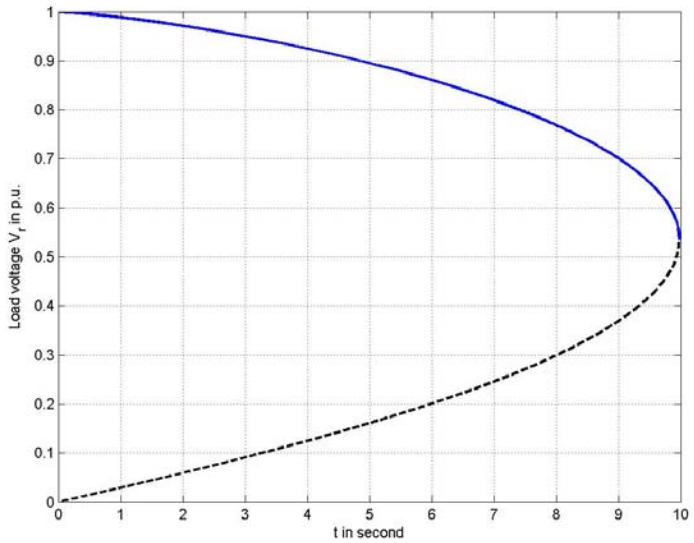

Figure 5.8 Possible load voltage Vr for the system in Example 5.1

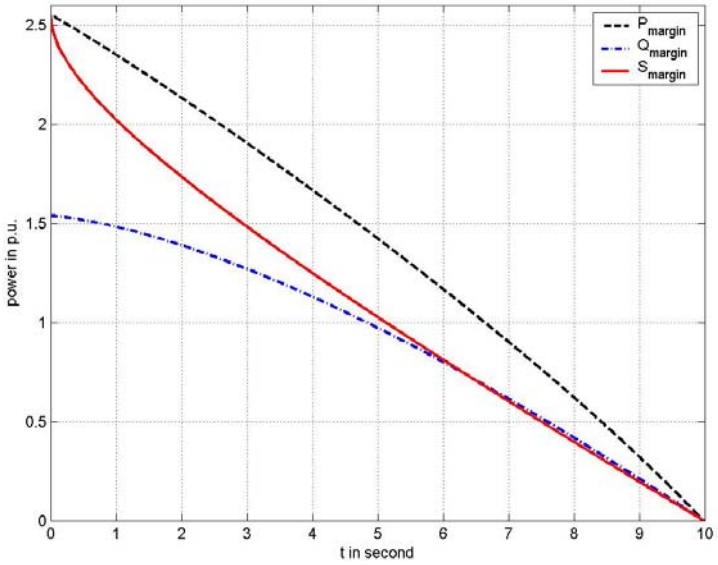

Figure 5.9 Three predicted load margins of the system in Example 5.1

5.2.3 *Voltage stability indices of single line system*

With the calculated load margins and the measurements of the current load demand, three voltage stability indices can be devised as shown in Equations 5.18 – 5.20. All three voltage stability indices range between 0 and 1. They decrease to 0 as the load demand increases to the maximum transferable power. Among the three voltage stability indices, the complex power based VSI_S is the minimum point where the load demand is inductive. Figure 5.10 shows the three voltage stability indices of Example 5.1. The voltage stability index of the single line system is defined as $VSI = min\{VSI_P, VSI_Q, VSI_S\}$.

$$VSI_P = \frac{P_{margin}}{P_{max}} \tag{5.18}$$

$$VSI_Q = \frac{Q_{margin}}{Q_{max}} \tag{5.19}$$

$$VSI_S = \frac{S_{margin}}{S_{max}} \tag{5.20}$$

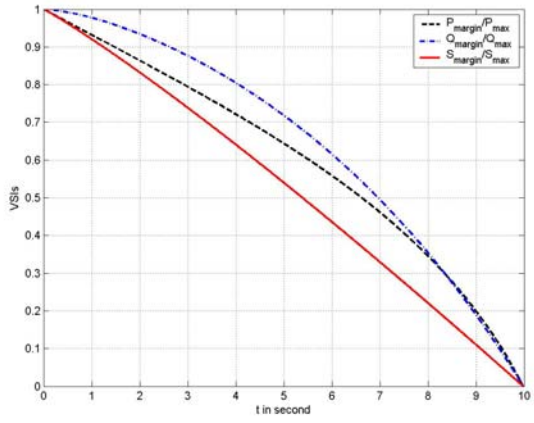

Figure 5.10 Voltage stability indices for the system in Example 5.1

5.3 Voltage stability index of a large power system

5.3.1 Power system partition

Electric power systems are interconnected together as the resulting larger system has better regulating characteristics. A disturbance happening to any of the subsystems is assimilated by the entire interconnected system and, therefore, the impact of the disturbance is mitigated. Nevertheless, the operational management and network analysis of the entire interconnected power system is a formidable task. Normally the interconnected power system is partitioned into three subsystems: the internal system (system of interest), the boundary system (buffer system), and the external system as illustrated by Figure 5.11.

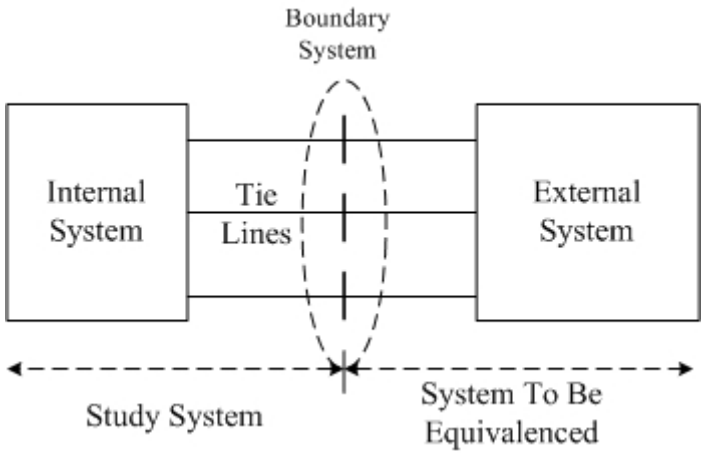

Figure 5.11 Interconnected power system

The boundary system is selected so that the external system is electrically separated from the internal system and the mutual impact between the internal system and external system is insignificant. The detailed model of the boundary system has to be

maintained as it has a significant impact on the internal system. The boundary system can be properly established through off-line contingency analysis or sensitivity analysis [56]. Normally, long EHV transmission lines connecting two areas serve as good candidates for the boundary system. With the designated boundary system, the external system can be largely unobservable and its structure need not be maintained and, therefore, can be represented by an equivalent system connected to the buses of the boundary system. Figure 5.12 illustrates the equivalent power system based on the extended Ward method, which substitutes the external system with artificial shunt branches and voltage sources attached to these boundary buses. A simpler representation of the external system is modeling the boundary buses as PV buses with power injection equal to the real-time measurement, as shown in Figure 5.13. This approach is similar to modeling a power flow slack bus, which is modeled as a PV bus with infinite generation capacity in conventional power flow analysis.

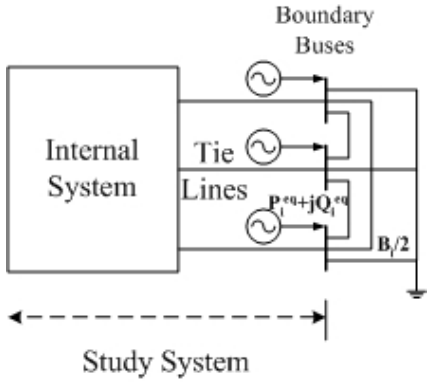

Figure 5.12 Equivalent interconnected power system (extended Ward method)

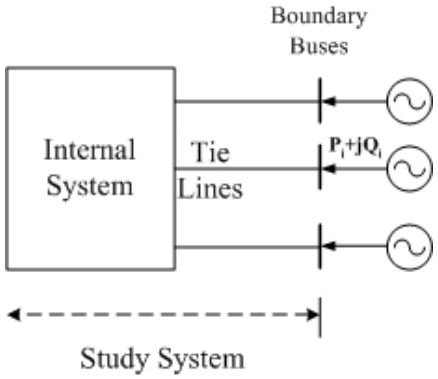

Figure 5.13 Equivalent interconnected power system (PV bus)

In fact, the difference between these two equivalent methods will not affect the results of the proposed VSI, is shown in the next section, where the shunt branches connected to these boundary buses are not part of the calculation. Therefore, these boundary buses are simply modeled as PV buses in this proposed voltage stability assessment method.

5.3.2 Power system network simplification

For a generic multi-bus power system, the current injection to each bus can be calculated by solving Equation 5.21, where V_{sys} is the complex bus voltage vector, Y_{sys} is the system network admittance matrix, and I_{sys} is the complex bus current injection vector.

$$I_{sys} = Y_{sys} \cdot V_{sys} \tag{5.21}$$

All the power system buses can be classified into three categories: 1) load bus, 2) tie bus, and 3) source bus. Load bus refers to the bus with any load attached. Tie bus refers to the bus with no load or any power generation device attached. Source bus

includes the generator bus, whose voltage is regulated by the attached generator, and the boundary bus, which is modeled as a PV bus. A source bus becomes a load bus if its attached generator reaches its capacity limit and loses its voltage regulation capability. By reordering Equation 5.21 based on the bus type, Equation 5.22 can be obtained.

$$\begin{bmatrix} I_L \\ I_T \\ I_G \end{bmatrix} = \begin{bmatrix} Y_{LL} & Y_{LT} & Y_{LG} \\ Y_{TL} & Y_{TT} & Y_{TG} \\ Y_{GL} & Y_{GT} & Y_{GG} \end{bmatrix} \begin{bmatrix} V_L \\ V_T \\ V_G \end{bmatrix} \tag{5.22}$$

By using the current injection of the load bus and tie bus and the voltage of the source bus, Equation 5.23 can be used to solve the voltage of the load bus and the tie bus and the current injection of the source bus.

$$\begin{bmatrix} V_L \\ V_T \\ I_G \end{bmatrix} = \begin{bmatrix} Z_{LL} & Z_{LT} & H_{LG} \\ Z_{TL} & Z_{TT} & H_{TG} \\ A_{GL} & A_{GT} & K_{GG} \end{bmatrix} \begin{bmatrix} I_L \\ I_T \\ V_G \end{bmatrix} \tag{5.23}$$

where

$$Z_{LL} = (Y_{LL} - Y_{LT} \cdot Y_{TT}^{-1} \cdot Y_{TL})^{-1} \tag{5.24}$$

$$Z_{LT} = -Z_{LL} \cdot Y_{LT} \cdot Y_{TT}^{-1} \tag{5.25}$$

$$H_{LG} = Z_{LL} \cdot (Y_{LT} \cdot Y_{TT}^{-1} \cdot Y_{TG} - Y_{LG}) \tag{5.26}$$

$$Z_{TT} = (Y_{TT} - Y_{TL} \cdot Y_{LL}^{-1} \cdot Y_{LT})^{-1} \tag{5.27}$$

$$Z_{TL} = -Z_{TT} \cdot Y_{TL} \cdot Y_{LL}^{-1} \tag{5.28}$$

$$H_{TG} = Z_{TT} \cdot (Y_{TG} - Y_{TL} \cdot Y_{LL}^{-1} \cdot Y_{LG}) \tag{5.29}$$

$$A_{GL} = Y_{GL} \cdot Z_{LL} + Y_{GT} \cdot Y_{TL} \tag{5.30}$$

$$A_{GT} = Y_{GT} \cdot Z_{LT} + Y_{GT} \cdot Z_{TT} \tag{5.31}$$

$$K_{GG} = Y_{GL} \cdot H_{LG} + Y_{GT} \cdot H_{TG} + Y_{GG} \tag{5.32}$$

As with the tie bus with zero current injection, the voltage of the load bus can be expressed by Equation 5.33.

$$V_L = Z_{LL} \cdot I_L + H_{LG} \cdot V_G \tag{5.33}$$

It is worth noting that the reference direction of these currents shown in Equation 5.23 is flowing towards the network. For the load bus, the load power direction is normally referred to as flowing out of the network. Therefore, the injection current to the i^{th} load bus can be expressed by Equation 5.34, where the complex power, S_i, is flowing out of the network and * stands for the conjugate operator.

$$I_i = \left(\frac{-S_i}{V_i} \right)^* \tag{5.34}$$

Replacing the I_i in Equation 5.34, we can get Equations 5.35 and 5.36. Equation 5.35 calculates the voltage of the j^{th} load bus, where N is the number of load buses and M is the number of source buses. By rearranging Equation 5.36, we get Equation 5.37, which matches the power flow calculation of the single source power system as shown in Figure 5.14. The V_{equ} and Z_{equ} of Figure 5.14 are shown by Equations 5.38 and 5.39.

$$V_{L_j} = \sum_{i=1}^{N} Z_{LL_{ji}} I_{L_i} + \sum_{k=1}^{M} H_{LG_{jk}} V_{G_k} \tag{5.35}$$

$$V_{L_j} = Z_{LL_{jj}} \left(\frac{-S_{L_j}}{V_{L_j}} \right)^* + \sum_{i=1, i \neq j}^{N} Z_{LL_{ji}} \left(\frac{-S_{L_i}}{V_{L_i}} \right)^* + \sum_{k=1}^{M} H_{LG_{jk}} V_{G_k} \tag{5.36}$$

$$\left(\frac{\sum_{k=1}^{M} H_{LG_{jk}} V_{G_k} - \sum_{i=1, i\neq j}^{N} Z_{LL_{ji}} \left(\frac{S_{L_i}}{V_{L_i}} \right)^* - V_{L_j}}{Z_{LL_{jj}}} \right)^* \cdot \left(V_{L_j} \right) = S_{L_j} \tag{5.37}$$

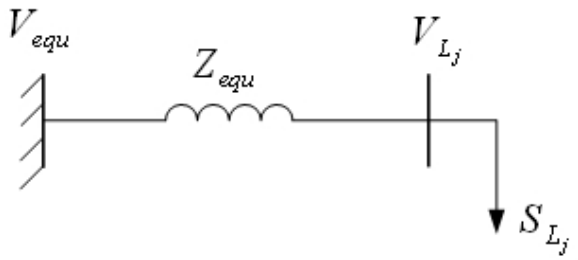

Figure 5.14 Derived equivalent single source power system

$$V_{equ_j} = \sum_{k=1}^{M} H_{LG_{jk}} V_{G_k} - \sum_{i=1, i\neq j}^{N} Z_{LL_{ji}} \left(\frac{S_{L_i}}{V_{L_i}} \right)^* \tag{5.38}$$

$$Z_{equ_j} = Z_{LL_{jj}} \tag{5.39}$$

The load power and load voltage of the original large power system are preserved in the derived equivalent circuit. Therefore, we can analyze the voltage stability based on this equivalent circuit, as the load power and load voltage are the two most important factors affecting the voltage stability. The following observations can be made from this derived equivalent circuit:

- The equivalent voltage source, V_{equ}, is a function of the true voltage sources and other system loads.
- The magnitude of the equivalent voltage source decreases as other system loads increase.

- The equivalent impedance, Z_{equ}, only depends on the system topology and line characteristics. To a power system with a fixed topology, the equivalent impedance remains constant.

Example 5.2

A simple three-bus power system, as shown in Figure 5.15, is used to illustrate the network simplification procedure. The network equation of this power system can be expressed by Equation 5.E.1. The calculated Z_{LL} and H_{LG} are given by Equation 5.E.2 and 5.E.3 respectively. The corresponding V_{equ} and Z_{equ} of the three-bus power system are given by Equations 5.E.4 and 5.E.5, respectively.

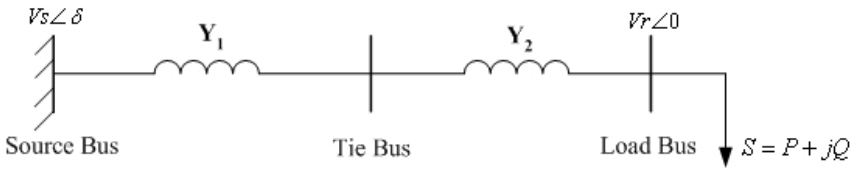

Figure 5.15 A three-bus power system of Example 5.2

$$\begin{bmatrix} I_L \\ I_T \\ I_G \end{bmatrix} = \begin{bmatrix} Y_2 & -Y_2 & 0 \\ Y_2 & Y_1+Y_2 & -Y_1 \\ 0 & -Y_1 & Y_1 \end{bmatrix} \begin{bmatrix} V_L \\ V_T \\ V_G \end{bmatrix} \quad (5.E.1)$$

$$Z_{LL} = \frac{1}{Y_1} + \frac{1}{Y_2} \quad (5.E.2)$$

$$H_{LG} = 1 \quad (5.E.3)$$

$$V_{equ} = V_s \angle \delta \quad (5.E.4)$$

$$Z_{equ} = Z_{LL} = \frac{1}{Y_1} + \frac{1}{Y_2} \quad (5.E.5)$$

5.3.3 *Large margin and VSI of a large power system*

After obtaining the derived equivalent single source circuit of the j^{th} load bus, as shown in Figure 5.15, Equations 5.9 – 5.17 can be used to calculate the load margin of this load bus. Similarly, Equations 5.40 – 5.43 show the calculated load margin of this load bus, where V_{equ_j} and Z_{equ_j} are shown in Equations 5.38 and 5.39, R_j and X_j are the real part and the imaginary part of the Z_{equ_j} respectively, and P_j, Q_j and θ_j are the j^{th} load characteristics.

$$P_{max_j} = \frac{Q_j \cdot R_j}{X_j} - \frac{\left|V_{equ_j}\right|^2 \cdot R_j}{2X_j^{\,2}} + \frac{\left|Z_{equ_j}\right| \cdot \left|V_{equ_j}\right| \cdot \sqrt{\left|V_{equ_j}\right|^2 - 4Q_j \cdot X_j}}{2X_j^{\,2}} \tag{5.40}$$

$$Q_{max_j} = \frac{P_j \cdot X_j}{R_j} - \frac{\left|V_{equ_j}\right|^2 \cdot X_j}{2R_j^{\,2}} + \frac{\left|Z_{equ_j}\right| \cdot \left|V_{equ_j}\right| \sqrt{\left|V_{equ_j}\right|^2 - 4P_j \cdot R_j}}{2R_j^{\,2}} \tag{5.41}$$

$$S_{max_j} = \frac{\left|V_{equ_j}\right|^2 \cdot \left[\,\left|Z_{equ_j}\right| - \left(\sin(\theta_j) \cdot X_j + \cos(\theta_j) \cdot R_j\right)\right]}{2\left(\cos(\theta_j) \cdot X_j - \sin(\theta_j) \cdot R_j\right)^2} \tag{5.42}$$

Accordingly, the VSI of each individual load bus is defined as shown by Equation 5.43. The VSI of the overall system is defined as Equation 5.44, where L is the number of load buses.

$$VSI_i = min\left\{\frac{P_{max_i} - P_i}{P_{max_i}}, \frac{Q_{max_i} - Q_i}{Q_{max_i}}, \frac{S_{max_i} - S_i}{S_{max_i}}\right\} \tag{5.43}$$

$$VSI_{sys} = \min_{i \in L}\left\{VSI_i\right\} \tag{5.44}$$

As voltage instability normally starts from local areas, different load buses may have different VSI values. The load bus with the minimum VSI has the smallest load

margin and is the closest to the voltage marginally stable point. Also the voltage stability margins of system load buses are mutually dependent as shown in Equation 5.39. The load increment at any load bus decreases the load margins of its neighboring load buses.

5.4 Measurement requirements for the proposed VSI

To apply the proposed VSI, the power system needs to be properly partitioned into the internal system, the boundary system, and the external system. Based on Equation 5.38 and 5.39, the time-synchronized measurements required by the proposed algorithm are summarized as follows:

- Voltage phasor of boundary buses, internal system generator buses, and internal system load buses
- Complex power or injection current of load buses and buses with generator connected (the complex power can be calculated by knowing the bus voltage and injection current) and
- Status of the devices, such as circuit breaker and capacitor bank, which are included as a part of the network model.

5.5 Practical implementation of the VSI

To implement the proposed VSI, the system network model (for example the network admittance matrix) of the internal system and the boundary system has to be made available in addition to these required time-synchronized measurements. If any time-synchronized device status measurement changes, the network model should be updated accordingly. For example, the line tripping indicated by the open status of its

circuit breakers requires the corresponding line admittance to be removed from the network admittance matrix. If the shunt capacitor bank is not modeled as a load whose power is measured, the switching on or off of the shunt capacitor bank requires the fixed admittance of the capacitor bank to be added to or removed from the network admittance network, respectively. If an ULTC transformer is modeled as part of the network model instead of being modeled as a part of an aggregated load, its tap change position has to be measured and used to update the corresponding network admittance elements.

The type of bus to which a generator is attached changes from a source bus to a load bus when the attached generator reaches its capacitor limit and loses its capability of voltage regulation. Detection of a generator reaching its capacitance limit can be achieved either through an indication signal sent from the generator OXL or by detecting its terminal voltage below the voltage regulation setting. A change of bus type triggers an update of the Z_{LL} and H_{LG} matrices. Figure 5.16 illustrates the functional diagram of the proposed VSI implementation.

5.6 Summary

In this chapter, the algorithm derivation of the proposed VSI was presented. It started with deriving the VSI of a simple power system taking the load power factor into consideration. Then a method of simplifying the large network behind a single load bus into a single voltage source and a single line was presented. With the simplified model, the VSI of the load bus can be directly calculated. Finally the data requirements and function procedure diagram was presented.

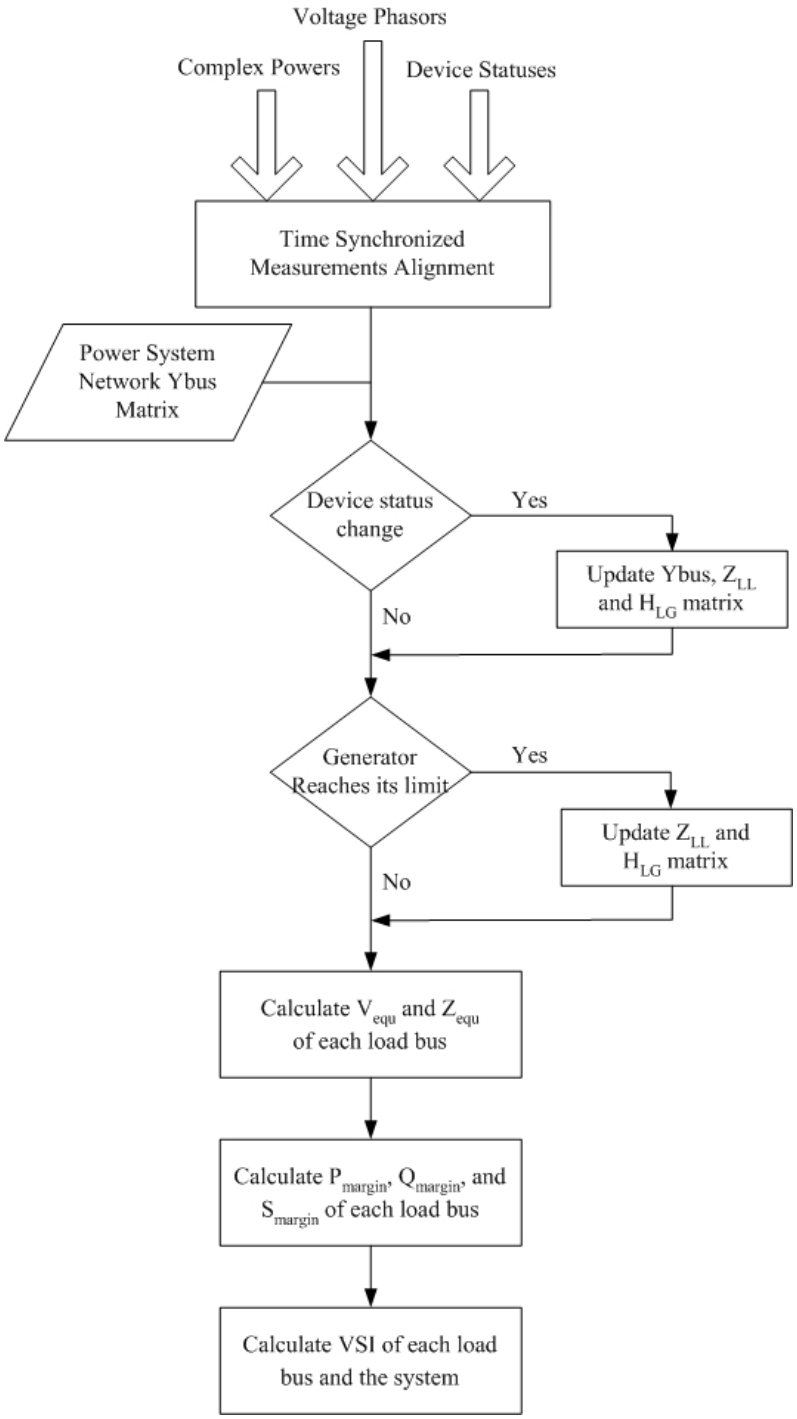

Figure 5.16 Functional diagram of the proposed VSI implementation

CHAPTER VI

PROPOSED VSI APPLICATION IN POWER SYSTEMS

6.1 Introduction

In Chapter 5, a new voltage stability index (VSI) based on the predicted load margin of each load bus has been proposed, and the result of applying the VSI on a simple two-bus power system model has been demonstrated. In this chapter, the proposed VSI will be examined on three widely tested power system models with larger sizes: the BPA 10-bus system, the IEEE 30-bus system [57], and the CIGRE 32-bus system [16]. The BPA 10-bus system will be studied through both steady state power flow analysis and time based dynamic simulation. The IEEE 30-bus system and the IEEE 118-bus system are studied only through steady state power flow analysis as the data required by the dynamic simulation are not readily available. The steady state power flow analysis is conducted by two software packages: PowerWorld Simulator and Power System Simulator for Engineering (PSS/E). The Power Systems CAD (PSCAD) simulation package, which is based on the well tested EMTDC solution engines, is used to carry out the time based dynamic simulation. The VSI functions are implemented in MATLAB m-files. The data exchange routine between the simulation packages and the MATLAB m-files were developed. The details about each test case and the test results are presented in each section.

6.2 BPA 10-bus test system

The BPA 10-bus test system, as shown in Figure 6.1, is originally described in [46] and is named as the BPA test system because it was constructed based on a part of the Bonneville Power Administration (BPA) power system. The test case with small variations has been broadly used to demonstrate and analyze the various aspects of voltage instability [2,4].

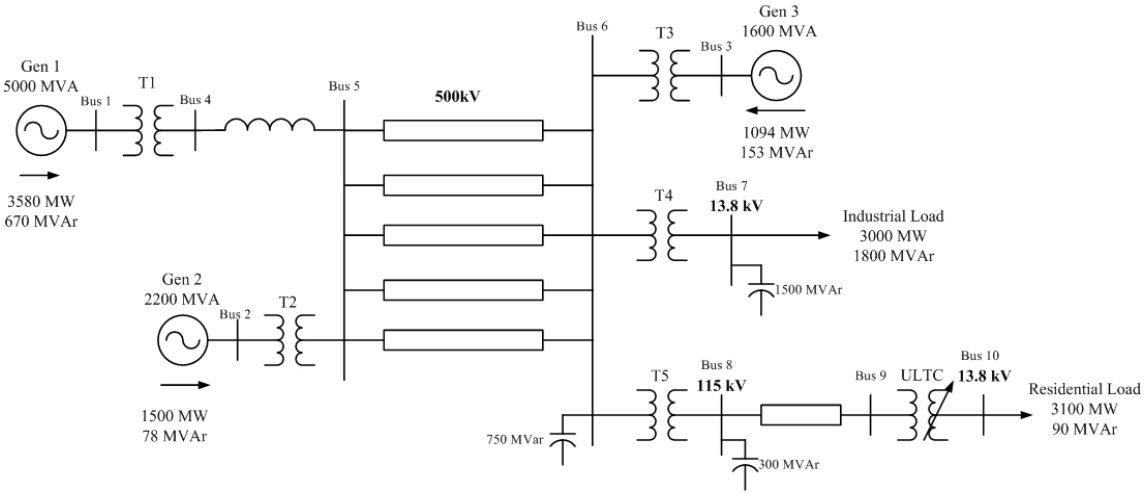

Figure 6.1 BPA 10-bus test system one-line diagram [2]

In this test system, two generators supply approximately 5000 MW to the load area, which consists of one aggregated industrial load and one aggregated residential load, through five 500-kV transmission lines. The load area has a generator, Gen 3, supplying a part of the load demand and regulating the load area voltage under normal conditions. The load area is heavily var-compensated by three large shunt capacitor banks. The capacity limits of the three generators are listed in Tab. 6.1. The industrial load is modeled as a constant power load. Fifty percent of the residential load is a

constant current load and the other fifty percent is a constant impedance load. The residential load is served by a ULTC transformer, which automatically regulates the low side voltage through changing the tap position at the high voltage side. The major cause of the voltage collapse is the outage of one 500-kV transmission line, followed by the ULTC operations to restore the residential load voltage.

Table 6.1 Generator capacity limits of the BPA 10-bus system

	Generator 1	Generator 2	Generator 3
Maximum MW	**5000**	**2200**	**1600**
Maximum MVar	**2000**	**700**	**400**

6.2.2 Steady state power flow analysis

The PowerWorld Simulator is used to carry out the steady state power flow analysis of this test case. As indicated by the term steady state, the results obtained are not a function of time. The line outage and ULTC tap changes are inputted manually. After each operation, the power flow algorithm is run to obtain the power flow results, including the bus voltage phasors. Then the power system admittance matrix and bus voltages are outputted to the VSI function, which is coded in MATLAB m-files, to obtain the voltage stability index of each load bus. Table 6.2 lists the bus voltages magnitudes in per unit before and after line outage. Before the line outage, the ULTC tap change position is at 0.95626 and no generator has reached its capacity limit. After the line outage, the generator Gen 3 reaches its capacity limit and loses its voltage regulation capability. Therefore, its terminal voltage (Bus 3) drifts below its voltage regulation setting, as shown in Tab. 6.2. Meanwhile, the residential load (Bus 10) voltage is below

its minimum voltage setting and, as a result, the ULTC starts to decrease its tap position at the primary side with a step size of 0.00626 to boost its secondary side voltage to the range of 0.99 to 1.01 *pu*. The generator, Gen 2, reaches its capacity limit when the ULTC tap position reaches the position of 0.91250. After changing the UTLC transformer tap position from 0.90625 to 0.9000, the power flow fails to converge and the system reaches its maximum loading point as well as the voltage marginally stable point. The results of the proposed VSI corresponding to system operation condition change are listed in Tab. 6.3. Assuming one of the 500kV transmission lines is opened after 5 seconds and the ULTC operation time delay is five seconds, the results of the VSI and ULTC tap position as functions of time are plotted in Figure 6.2. Fig 6.3 shows the voltage magnitudes of bus 6, load bus 7, and load bus 10. Bus 10 voltage is maintained relatively stable due to the ULTC operation during the process.

Table 6.2 BPA test system bus voltages in p.u. (before and after line outage)

Bus #	1	2	3	4	5	6	7	8	9	10
Before	0.980	0.965	0.972	1.096	1.088	1.070	1.000	0.999	0.957	1.000
After	0.980	0.965	0.950	1.092	1.073	1.031	0.959	0.962	0.921	0.960

Based on the results shown in Tab. 6.3, we can observe that the proposed VSI is able to detect accurately the voltage instability. After 40 seconds, the VSIs of both load buses become very close to zero, which indicates the system is approaching the marginally stable point. After one more tap change operation of the UTLC transformer at 45 seconds, any further attempt to restore the load through ULTC tap change operation

causes the power system voltage collapse, which is indicated by the power flow failure to converge.

Table 6.3 VSI outputs of the BPA test system based on steady state analysis

		Proposed VSI	
		Bus 7	Bus 10
Before Line Outage		0.4285	0.3484
After Line Outage		0.0646	0.0775
ULTC Tap Position	**0.95000**	0.0613	0.0733
	0.94375	0.0581	0.0692
	0.93750	0.0547	0.0652
	0.93125	0.0513	0.0611
	0.92500	0.0479	0.0571
	0.91875	0.0444	0.0532
	0.91250	0.0007	0.0001
	0.90625	0.0046	0.0001

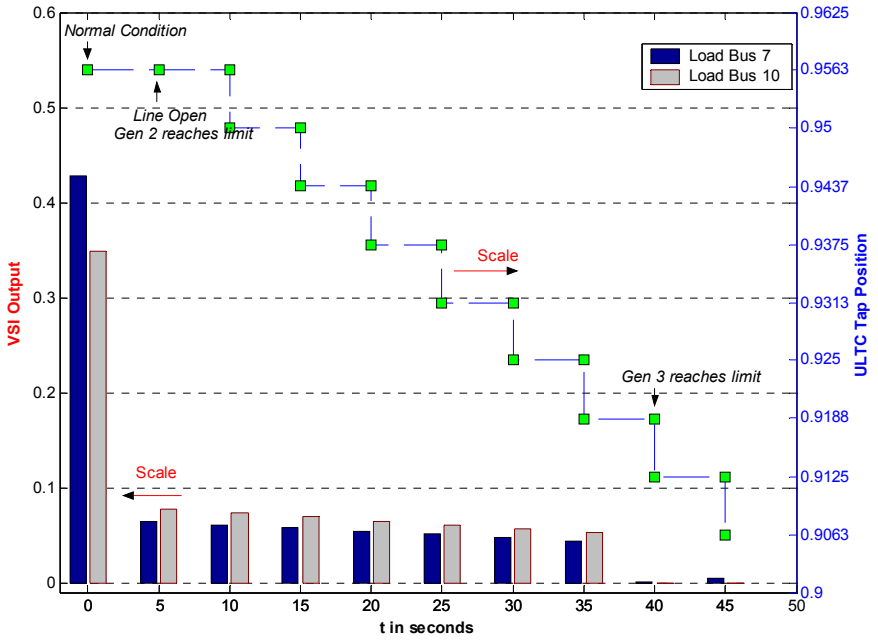

Figure 6.2 Proposed VSI of the BPA test system (from steady state analysis)

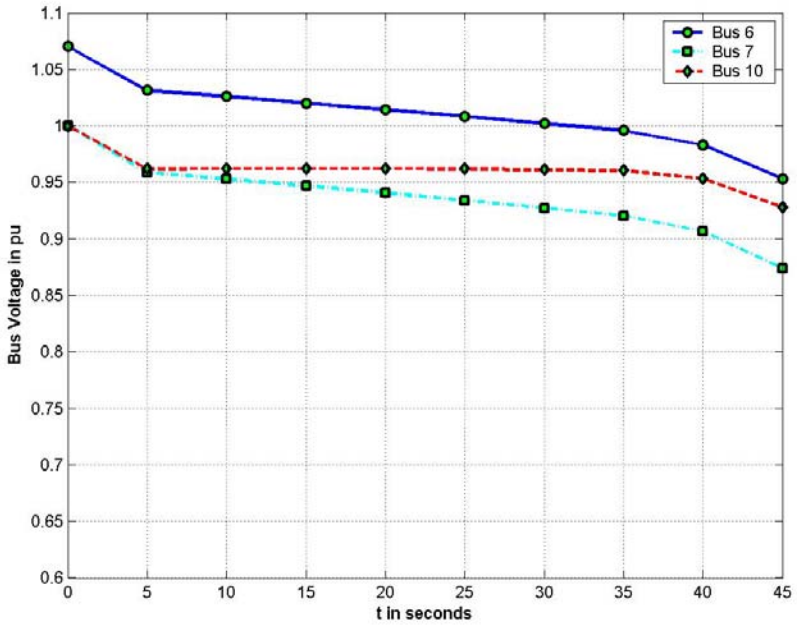

Figure 6.3 Bus voltages of BPA test system (from steady state analysis)

6.2.3 Time based dynamic simulation

The BPA test system is modeled in PSCAD with the same transmission line and transformer parameters as used in the steady state power flow analysis. Typical synchronous generator parameters and standard static excitation systems, which are not modeled by the steady state power flow algorithm, are used to fulfill the requirements of time-based simulation. The excitation overcurrent limits are tuned to enforce the reactive power generation limits of Gen 2 and Gen 3 approximately as listed in Table 6.1. Voltage stability assessment related functions, as illustrated in Figure 5.16, are implemented in MATLAB m-files. An interface has been developed to facilitate the dynamic data

exchange between the PSCAD and the m-files at every simulation time step. The line is also opened after 5 seconds and the UTLC tap change operates with 5 seconds of delay.

Figure 6.4 shows the load margin and the VSI of the load bus 7. P_{max}, Q_{max}, and S_{max} are the three predicted maximum power demands. The P, Q, and S are the real-time measurements of the three corresponding load consumptions. These three predicted maximum power demands shrink notably when one of the five transmission lines opens at 5 seconds, and simultaneously merges with the respective power consumption at around 40 seconds when the system reaches the marginally stable point. The corresponding VSI is shown in the fourth plot of Figure 6.4. As the reactive power demand of this load bus is positive, the VSI based on the complex power remains as the minimum and, therefore, becomes the VSI of the load bus. Similarly, Figure 6.5 shows the load margin and VSI of the load bus 10. The VSIs of the two load buses and the ULTC transformer tap position are shown in Figure 6.6. Figure 6.7 shows the voltages of Bus 6, Bus 7, and Bus 10. As observed from Figure 6.7, the voltages of both buses drop dramatically at 50 seconds, which clearly indicates a voltage collapse.

Comparing the results shown in Figure 6.6 and Figure 6.10 shows that the results obtained from time-based dynamic simulations match very closely to the results obtained from the steady state analysis. Results from both analysis methods show that the proposed VSI can identify the voltage marginally stable point of each load bus and can provide the stability margin in a readable format.

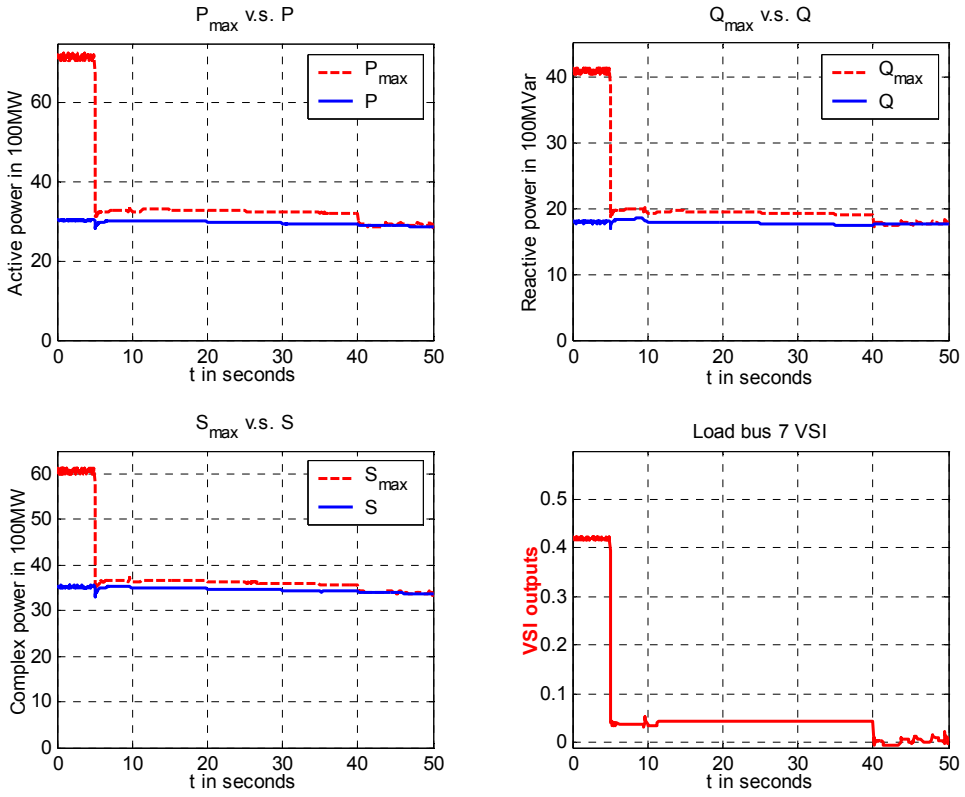

Figure 6.4 Load bus 7 load margin and VSI (from dynamic simulation)

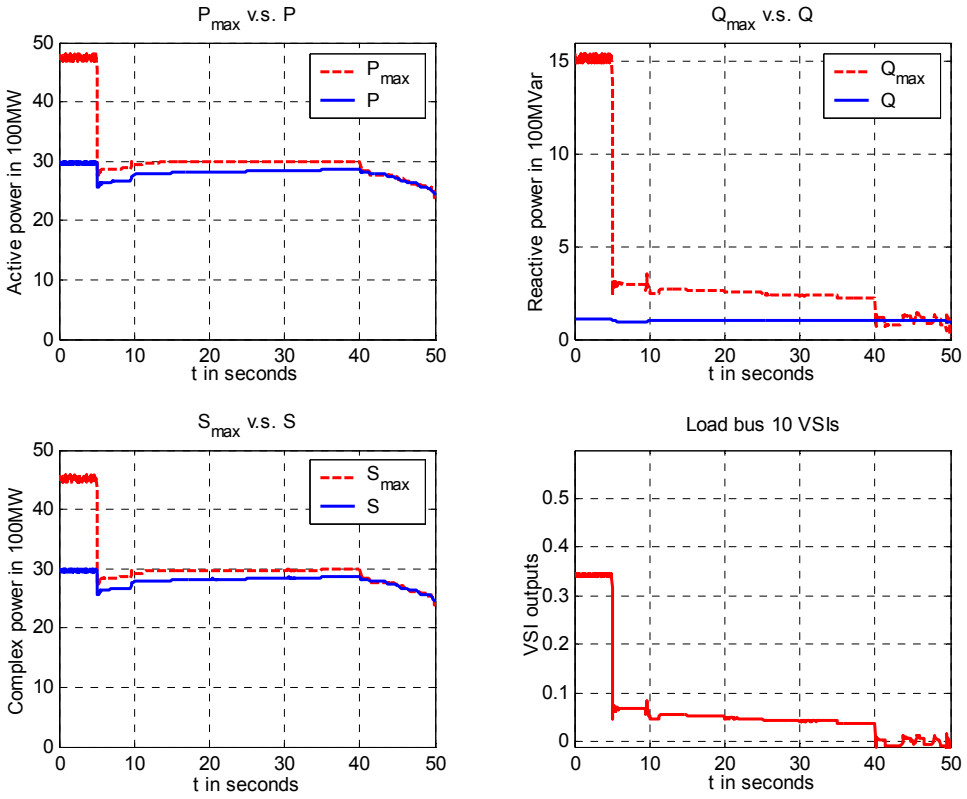

Figure 6.5 Load bus 10 load margin and VSI (from dynamic simulation)

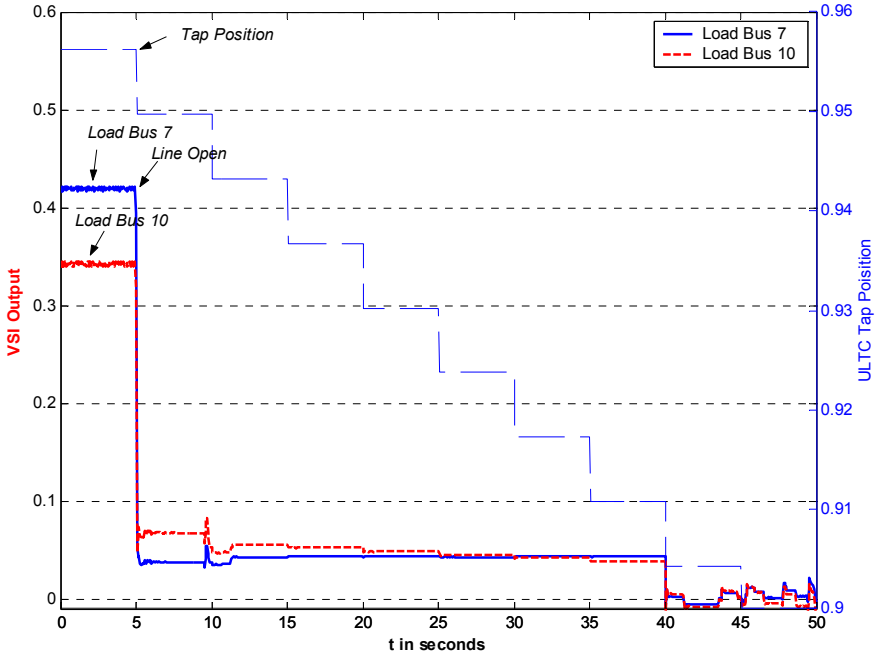

Figure 6.6 VSI of the BPA ten-bus system (from dynamic simulation)

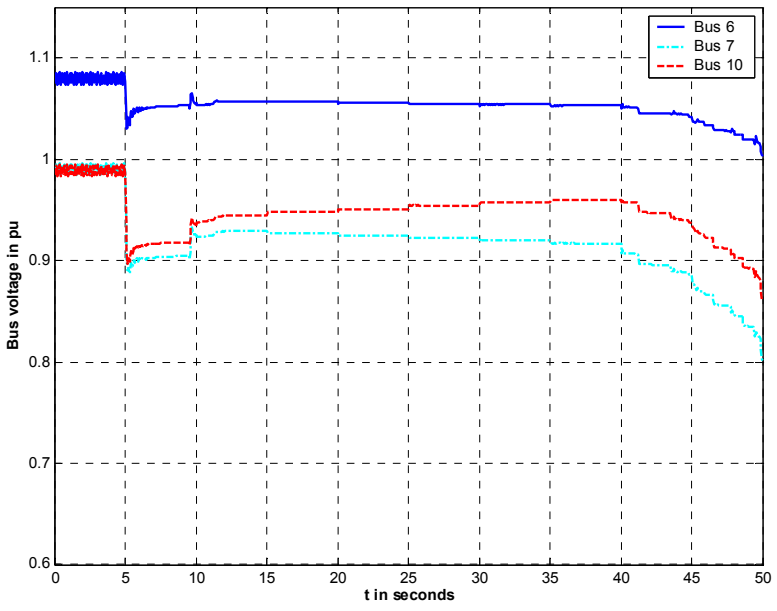

Figure 6.7 Bus voltages of BPA ten-bus system (from dynamic simulation)

6.3 IEEE 30-bus test system

The IEEE 30-bus test case is one of the widely used test cases available from the power system test case archive [57]. Figure 6.8 shows the one line diagram of the power system. The system mainly consists of two parts: a 33kV system and a 132kV system. The system reactive power support is largely from synchronous condensors. The 33kV system is heavily loaded and has loads attached at most of the buses. Under the normal conditions, as specified by the original test case data, bus 30 has the lowest voltage as it is farthest away from the source. The VSI application on this test case is conducted only through the steady state analysis, because the model information required by dynamic information is not available. Two types of tests are conducted to verify the applicability of the proposed VSI. First, the load of a bus that is not the most distant load bus from the source is increased until the power flow diverges. The second test is to increase simultaneously all the loads in steps of a fixed percentage of their respective initial load values with constant power factors maintained until the power flow diverges. Tab. 6.4 lists five load buses with the minimum VSI under the initial conditions. The system its under initial conditions is clearly distant from the voltage collapse, as the minimum VSI (0.7769) is much larger than 0 (voltage stability limit).

Table 6.4 Five load buses with the minimum VSI under the initial condition

Bus Number	30	26	21	24	19
VSI Output	0.7769	0.8769	0.8871	0.9106	0.9136

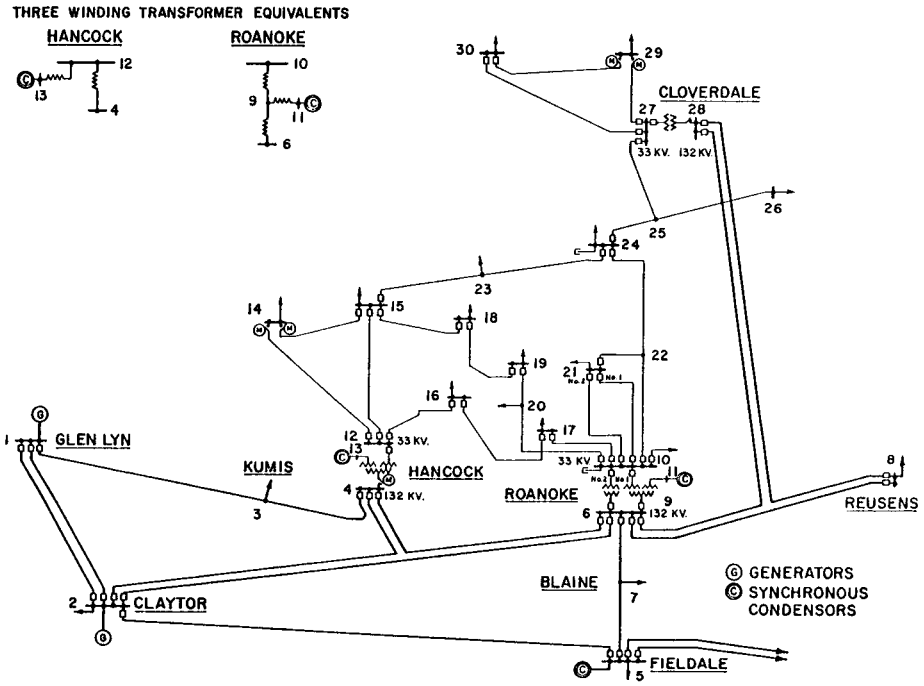

Figure 6.8 IEEE 30-bus test system one-line diagram [57]

6.3.2 Increase an individual load

The load at bus 10 is chosen to be increased as bus 10 is not among the buses with the minimum VSIs under the initial condition and it is not the most 'electrically' distant bus from the source. The VSIs of bus 10 and five other buses with the minimum VSIs under the initial conditions, as listed in Tab. 6.4, are plotted in Figure 6.9 as the complex power of the load at bus 10 ranges from zero to its maximum loading point with load factor as 0.945. From Figure 6.9 we can observe that the proposed VSI not only accurately detects the voltage marginally stable point of each individual load bus, but also correctly identifies the load bus that has the minimum load margin and is the most vulnerable to voltage collapse.

Figure 6.10 shows the predicted maximum complex power loading point of bus 10 and the power consumption of bus 10. It can be observed that the initially predicted maximum complex power loading point, which is around 140 MVA, for load bus 10 is close to its final maximum load consumption (125MVA), causing the system to reach its voltage marginally stable point.

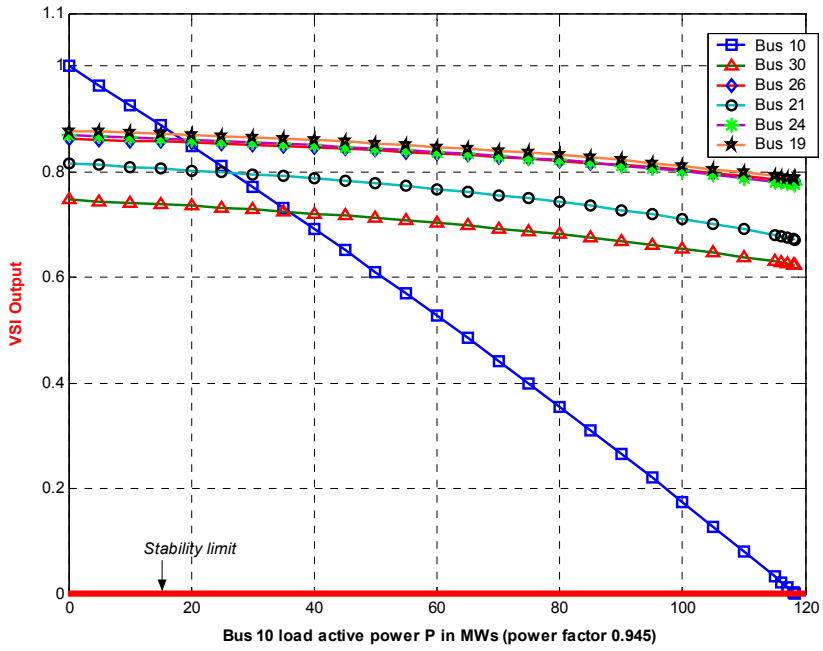

Figure 6.9 VSIs of selected load buses

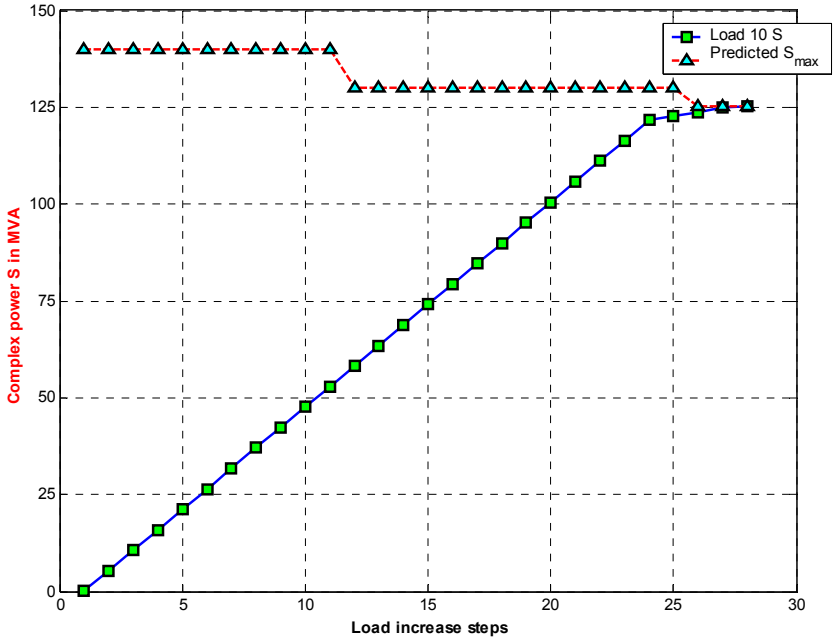

Figure 6.10 Predicted S_{max} of load bus 10

6.3.3 Increase all loads simultaneously

The system overall load under the initial condition is 283.40 MW for the active power and 126.20 MVar for the reactive power. All the loads are increased by the same scale factor with their own power factors maintained as constants. The power flow fails to converge as the system's overall load reaches 175% of the initial load. Figure 6.11 plots the five load buses with minimum VSIs (closest to the marginally stable point) when the power flow diverges. The proposed VSI identifies the load bus 30 as the most vulnerable load bus to voltage collapse. Figure 6.13 shows the predicted maximum complex power loading point, which decreases as other loads increases, and the complex power consumption of bus 30.

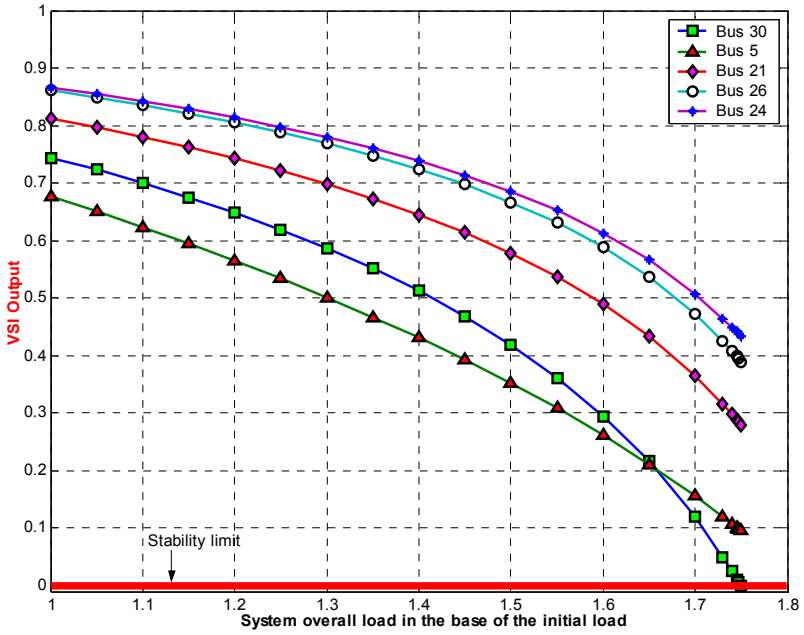

Figure 6.11 The five buses with the minimum VSIs (loads increased evenly)

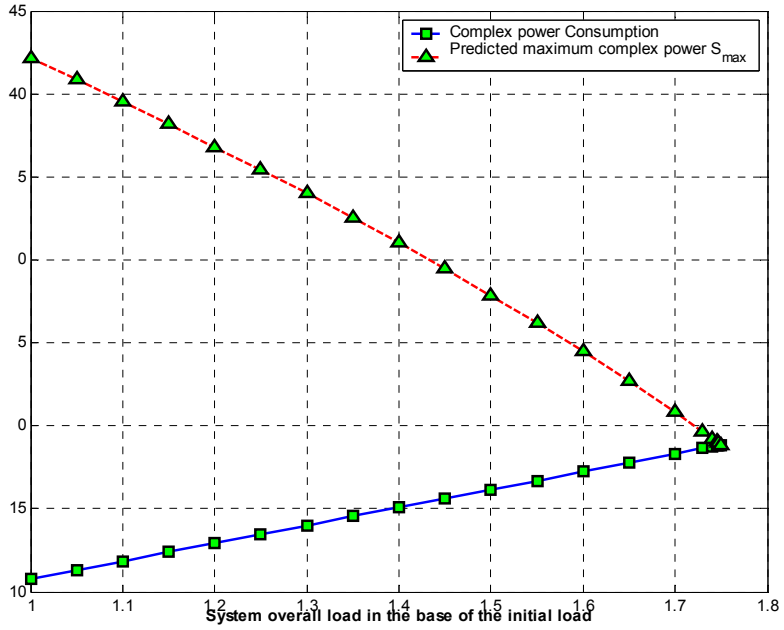

Figure 6.12 Predicted S_{max} of bus 30 (loads increased evenly)

6.4 CIGRE 32-bus test system

The 32-bus test system, as shown in Figure 6.13, is actually based on northern Belgium's power system, which experienced a voltage collapse in 1982. The test system mainly consists of three layers with different voltage levels. The interconnected 380kV layer, including equivalent external systems, has the generators that supply most of the power. The 150kV system has three connected generators, which deliver constant power (PQ bus) and have no voltage regulation capability under the initial conditions. The internal system loads connected to buses N201 through N207 at 70kV are fed from ULTC transformers connected to the 150kV system. The test system was first presented in a CIGRE's report [29] and later was used by other researchers[16]. The series of events that drove the system to collapse are summarized as the following [16,29].

- At 30 second, all the internal system loads start to increase steadily at the rate of 30% in 7200s with a constant ratio between P and Q. All other loads remain unchanged.
- The line connecting buses N16 and N3 is tripped at 5000s. The system is assumed to remain stable successfully after the event.
- The internal system load stops increasing at 7230s.
- Machine M2 is tripped off the system at 7400s, which causes the system voltage to collapse rapidly.

Steady state power flow calculations are used to conduct the simulation. The internal system loads are increased at a fixed step of 2.5%, which corresponds to 600

seconds of load incremental time. The line is tripped when the system load reaches 120.71%, which corresponds to 5000 s.

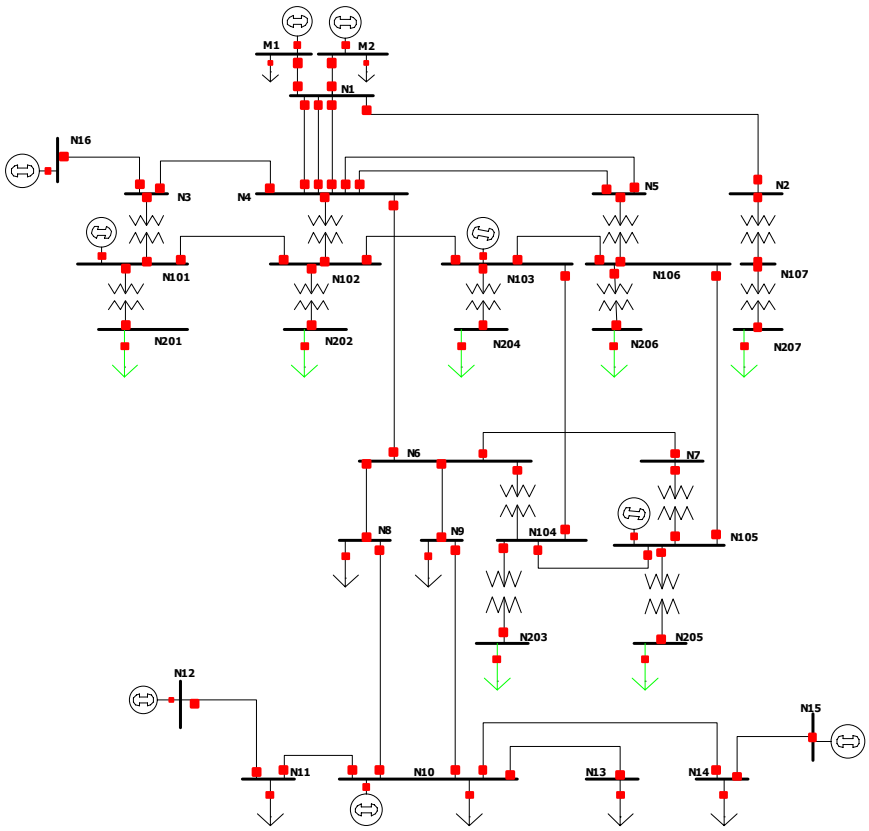

Figure 6.13 CIGRE 32-bus test system one-line diagram

Figure 6.14 shows the VSIs of the power system and two load buses (N201 and N207), which have the two minimum VSIs among the seven load buses of the internal system, before the machine M2 is tripped off at 7400s. It can be observed that the system VSI is already below 0.25, which indicates a small load margin exists, before the major generator M2 is tripped off. As one of the limitations of the power flow based steady state analysis, the power flow calculation does not converge at severe events that cause

system voltage collapse. In this case, the power flow solution as well as the VSI cannot be obtained as the power flow calculation diverges at the event of Machine M2 tripping.

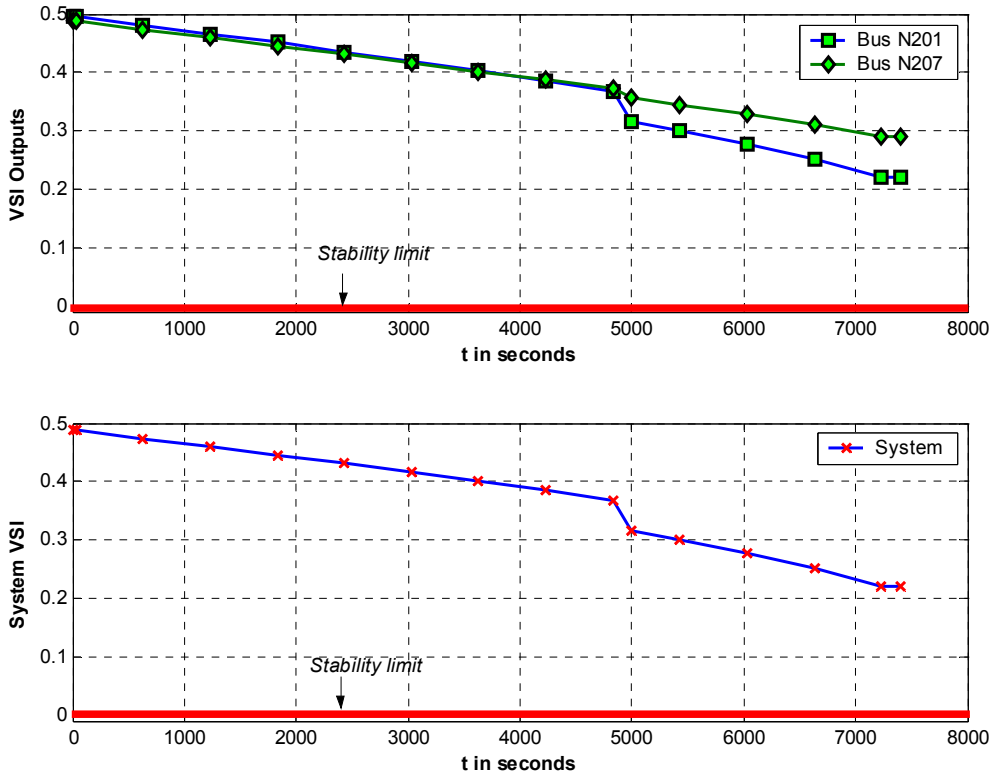

Figure 6.14 VSIs of the CIGRE 32-bus system

6.5 Results, analysis and discussion

In this chapter, the proposed VSI method was applied to practical power systems to demonstrate its applicability and performance in predicting the power system voltage stability margin and detecting the voltage marginally stable point. For the BPA 10-bus power system, where the voltage collapse is caused by a line outage and ULTC transformer operation, the results obtained from steady state analysis and time-based dynamic simulation match well and both demonstrate the accuracy of the VSI in detecting the voltage marginally stable point. The system reaches its marginally stable point when the predicted maximum loading point meets the load consumption and the index value of the load bus is very close to or equal to zero. Test results of applying the VSI on the IEEE 30-bus system have demonstrated that the VSI quickly identifies the load bus, which contributes the most to the system voltage collapse and has the minimum load margin, in addition to accurately detecting the system marginally stable point when the system loads are increased evenly.

As mentioned earlier in Chapter 5, boundary buses, which can be found through off-line simulation, with relatively stable voltages are normally approximated as voltage sources. But in reality, their voltages are not necessarily maintained as constants. Therefore, when the VSI is applied to real power systems, the maximum loading point may not exactly correspond to the system when the VSI equals zero, even though the source voltage magnitude is already taken into consideration by the VSI calculation. A small load margin, such as 5%, instead of a zero load margin is recommended to be used to declare when the system has reached its marginally stable point. Furthermore, for a

load bus with a larger percentage of induction motor load, the reactive power consumption increases dramatically when the bus voltage is drifting below the rated voltage but above the voltage where the motor loads are dropped. In order to allow remedial actions to have enough time to prevent voltage collapse, a 10% -20% load margin, which corresponds to 0.1 – 0.2 for the VSI, is a reasonable threshold for a load bus with a large portion of induction motor load.

The load margin estimated by the proposed VSI is based on the assumption of a steady load increment. No other contingency analysis, such as the event of machine M2 tripping in the CIGRE 32-bus test case, is considered by the VSI at this stage. Events that are not severe enough to cause rapid system collapse, such as the line outage that happened in the first test case, should not affect the performance of the proposed VSI. In order to increase the voltage stability margin and prevent a possible contingency from causing fast voltage collapse, a higher VSI threshold (larger load margin), such as 0.3 for this case, can be set to initiate preventive actions, such as switching in capacitor banks. The proper setting of the proposed VSI based load margin to prevent fast voltage collapse due to severe contingencies still needs careful off-line study. Different systems may need different load margins to withstand their severest contingencies.

The overall implementation of the proposed VSI is straightforward and the computational demand is affordable for on-line applications. As counting floating-point operations is no longer practical since MATLAB incorporates a new matrix computational method, the computational demand of the proposed VSI is measured in the time that a desktop computer with Intel Pentium IV 3.2GHz CPU and 1Gigabye memory

space takes to calculate the VSI of the system and all load buses. Tab. 6.5 lists the VSI computation times of the three test cases. These computational times were measured for scenarios in which the network topology is changed and, consequently, matrix updating is required. If the system network topology remains unchanged, the computation time will be further reduced.

Table 6.5 VSI computation time

BPA 10-bus System	**IEEE 30-bus System**	**CIGRE 32-bus System**
0.011 (second)	0.030 (second)	0.031 (second)

6.6 Summary

In this chapter, the developed VSI has been tested on three test cases. In the first test case, the VSI was verified through both steady state analysis and time-based dynamic simulation methods. Test results have validated the applicability and accuracy of the proposed VSI.

CHAPTER VII

CONCLUSIONS AND FUTURE WORK

7.1 Conclusions

Power system voltage instabilities are dynamic phenomena in which numerous nonlinear devices are involved. In order to make the assessment of power system voltage instability manageable, this research focused on the root cause of the voltage instability. That is, voltage collapse starts when the load demand surpasses the maximum power that can be generated and transferred to the load center. Given the time-synchronized measurements of power system variables, a method was derived to predict the maximum transferable active power, reactive power, and complex power, respectively, of the single source power system. Then a VSI was devised based on these load margins, which are the differences between the maximum transferable powers and the corresponding load consumption measurements. To apply the VSI to large power systems, a computationally efficient network reduction method was developed to simplify the power system behind each load bus into a single source and a single line model with the power and voltage of the load bus preserved. Then, the VSI of each load bus can be readily calculated from its simplified single source power model. The network simplification method and the devised VSI provide a new voltage stability assessment method for large power systems. Test results of applying the proposed voltage stability assessment method on three power systems have demonstrated that it has the following salient features:

- The proposed method can identify the system voltage marginally stable point with satisfactory accuracy.
- The proposed method provides system voltage security in the format of a load margin that is readable and informative.
- The proposed method can identify the load bus that is the most susceptible to voltage collapse.
- The proposed method is computationally efficient, and can be easily implemented to predict the voltage stability of large power systems in almost real time.

The main contribution of this dissertation is the development of a practical synchronized phasor measurement based voltage stability index that can accurately predict the power system voltage stability with affordable computational demands for on-line applications. The proposed voltage stability assessment method could be incorporated into wide area protection and control systems to monitor the power system voltage stability security. Also, the newly proposed network reduction method enables users to analyze the voltage stability of each load bus and design of distributed control schemes to prevent voltage collapse.

7.2 Future work

Although the proposed VSI can identify the voltage marginally stable point, a certain amount of load margins need to be maintained for the power system to withstand possible contingencies and to reduce the chance of voltage collapse. An investigation of

ways to incorporate the proposed VSI with on-line contingency analysis will improve the power system voltage stability security.

Furthermore, an investigation of applying the VSI to the following areas is recommended:

- Develop the proposed VSI based control scheme to control various reactive compensation devices, such as shunt capacitor banks, to maintain proper voltage security margins.
- Incorporate the proposed VSI output into the design of an optimal load shedding scheme.

REFERENCES

[1] North American Electric Reliability Council, "*NERC Recommendations to Prevent and Mitigate the Impacts of Future Cascading Blackouts,*" January. 2004.

[2] C. W. Taylor, **Power System Voltage Stability**, EPRI Power System Engineering Series, McGraw Hill, 1994.

[3] T. Van Cutsem and C. Vournas. **Voltage Stability of Electric Power Systems**. Kluwer Academic Publishers, 1998.

[4] Prahba Kundur, **Power System Stability and Control**, EPRI Power System Engineering Series, McGraw Hill, 1994.

[5] C.W. Taylor, D. C. Erickson, K. E. Martin, and V. Venkatasubramanian, "WACS-wide-area stability and voltage control system: R&D and online demonstration," *Proceedings of the IEEE*, Vol. 93, No. 5, pp. 892 – 906, May 2005.

[6] G. Benmouyal, E.O. Schweitzer, and A. Guzman, "Synchronized Phasor Measurement in Protective Relays for Protection, Control, and Analysis of Electric Power Systems," *Western Protection Relay Conference*, 29 Annual, October 2002.

[7] IEEE/CIGRE Joint Task Force on Stability Terms and Definitions. Definition and Classification of Power System Stability. *IEEE Transactions on Power Systems*, Vol. 19, No. 2, pp.1387-1401, May 2004.

[8] CIGRE Task Force 38-02-12, Criteria and Countermeasures for Voltage Collapse, *CIGRE Publication*, 1994.

[9] IEEE Working Group on Voltage Stability, Voltage Stability of Power System: Concepts, Analytical Tools, and Industry Experience, *IEEE Special Publication* 90TH0358-PWR, 1990.

[10] CIGRE Task Force 38-02-05, *Load Modeling and Dynamics*, Electra, pp.124-142, May 1990.

[11] IEEE Task Force, Load Presentation for Dynamic Performance Studies, *IEEE Transaction on Power Systems*, Vol. 8, No. 2, pp. 472-482, May 1993.

[12] IEEE Task Force, Standard Load Models for Power Flow and Dynamic Performance Simulation, *IEEE Transactions on Power Systems*. Vol. 10, No. 3, pp. 1302-1313, August 1995.

[13] D. Karlsson, D. J. Hill, "Modeling and Identification of Non-linear Dynamic Loads in Power Systems," *IEEE Transactions on Power Systems*, Vol. 9, No. 1, pp. 157-166, February 1994.

[14] W. Xu and Y. Mansour, "Voltage stability analysis using generic dynamic load models," *IEEE Transactions on Power Systems*, Vol. 9, No. 1, pp. 479-493, February, 1994.

[15] W.W. Price, Discussion of [14].

[16] IEEE Working Group on Power System Stability, Voltage Stability Assessment: Concepts, Practices and Tools, *IEEE Power System Stability Subcommittee Special Publication SP101PSS*, 2002.

[17] IEEE Standard Board. *IEEE Recommended Practice for Excitation System Models for Power System Stability Studies*. IEEE Standard. 1992.

[18] IEEE Task Force on Excitation Limiters, Recommended Models for Overexcitation Limiting Devices. *IEEE Transactions on Energy Conversion*, Vol. 10, No. 4, pp. 706-713, December 1995.

[19] T. Van Cutsem and C. Vournas, "Voltage stability analysis in transient and mid-term time scales," *IEEE Transactions in Power Systems*, Vol. 11, No. 1, pp. 146-154, February 1996.

[20] J. D. Glover, M. S. Sarma, **Power System Analysis and Design**, 3rd ed., Brooks/Cole, 2001.

[21] M. Crow, **Computational methods for electric power systems**, CRC Press, 2002.

[22] I. Dobson and H. D. Chiang, Towards a Theory of Voltage Collapse in Electric Power Systems, *System and Control Letter*, Vol.13, 1989.

[23] I. Dobson and L. Lu, "New Methods for Computing a Closest Saddle-node Bifurcation and Worst Case Load Power Margin for Voltage Collapse," *IEEE Transactions on Power Systems*, Vol.8, No. 3, pp. 905-103, August 1993.

[24] V. Ajjarapu and C. Christ, "The continuation power flow: a tool for steady state voltage stability analysis, " *IEEE Transactions on Power Systems*, Vol. 7, No. 1, , pp.416-423, February 1992.

[25] B. Gao, G. K. Morison, and P. Kundur, "Voltage Stability Evaluation Using Modal Analysis", *IEEE Transaction on Power Systems*, Vol.7, No. 4, pp. 1529-1542, November 1992.

[26] B. Gao, G. K. Morison, and P. Kundur, "Towards the Development of a Systematic Approach for Voltage Stability Assessment of Large-scale Power Systems," *IEEE Transaction on Power Systems*, Vol.11, No. 3, pp.1314-1324, August 1996.

[27] C. A. Canizares, A. Z. de Souza, and V.H. Quintana, "Comparison of performance indices for detection of proximity to voltage collapse," *IEEE Transactions on Power Apparatus and Systems*, Vol. 11, No. 3, pp. 1441-1450, August 1996.

[28] H.D. Chiang and R. Jean-Jumeau, "Toward a practical performance index for predicting voltage collapse in electric power systems," *Proceeding of the 1993 IEEE/PES Summer Meeting*, July 1993.

[29] CIGRE Task Force 38-02-11, Indices Predicting Voltage Collapse Including Dynamic Phenomena, *CIGRE Publication*, 1994.

[30] R. J. Thomas and A. Tiranuchit, "Voltage instabilities in electric power networks*," Proceedings of the 18th Southeastern Symposium on System Theory*, Apr. 1986, pp. 359-363.

[31] A. Tiranuchit and R. J. Thomas, "A posturing strategy against voltage instabilities in electric power system," *IEEE Transactions on Power Systems,* Vol. 3, No. 1, pp.87-93, February 1988.

[32] P. A. Löf, T. Smed, G. Andersson, and D. J. Hill, "Fast calculation of a voltage stability index," *IEEE Transactions on Power System*, Vol. 7, No. 1, pp. 54-64, February 1992.

[33] M. Suzuki and K. Masegi, "Direct calculation of voltage-stability limit of electric power systems," *Electrical Engineering in Japan*, Vol. 111, No. 7, pp. 40-48. 1991.

[34] C. Concordia, "Voltage stability simplified," *International Journal of Electrical & Energy Systems*, Vol. 14, No. 5, pp. 364-366, October 1992.

[35] M. M. Begovic and A.G. Phadke, "Control of voltage stability using sensitivity analysis," *IEEE Transactions in Power Systems*, Vol. 7, No. 1, pp. 114-123, February 1992.

[36] Y. Tamura, H. Mori, and S. Iwamoto, "Relationship between voltage instability and multiple load flow solutions in electric power systems," *IEEE Transactions on Power Apparatus and Systems*, vol. 102, no. 5, pp. 1115-1125, May 1983.

[37] Y. Tamura, K. Sakamoto, and Y. Tayama, "Current issues in the analysis of voltage instability phenomena," *Proc. Bulk Power System Phenomena – Voltage Stability and Security*, EPRI, pp.5-39, January 1989.

[38] P. Kessel and H. Glavitsch, "Estimating the voltage stability of a power system," *IEEE Transactions on Power Systems*, Vol. 1, No. 3, July 1986, pp. 346-354.

[39] T. Q. Tuan, J, Fandino, N. Hadjsaid, J. C. Sabonnadiere, H. Vu, "Emergency load shedding to avoid risks of voltage instability using indicators," *IEEE Transactions on Power Systems*, Vol. 9, No. 1, pp. 341-351, February 1994.

[40] K. Vu, M. Begovic, D. Novosel, and M. Saha, "Use of local measurements to estimate voltage-stability margin," *IEEE Transactions on Power Systems*, Vol. 14, No. 3, pp. 1029-1035, August 1999.

[41] B. Milosevic and M. Begovic, "Voltage-Stability Protection and Control Using a Wide-Area Network of Phasor Measurement," *IEEE Transactions on Power Systems*, Vol. 18, No. 1, pp. 121-127, February 2003.

[42] V. Ajjarapu and C. Christ, "The continuation power flow: a tool for steady state voltage stability analysis, " *IEEE Transactions on Power Systems*, Vol. 7, No. 1, pp.416-423, February 1992.

[43] N. Yorina, S. Harada, and H. Cheng, "A method to approximate a closest loadability limit using multiple load flow solutions," *IEEE Transactions on Power Systems*, Vol. 12, No. 1, pp. 424-429, February, 1997.

[44] T. Van Cutsem, "A method to compute reactive power margins with respect to voltage collapse," *IEEE Transactions in Power Systems*, Vol. 6, No. 1, pp. 145-156, February 1991.

[45] C. A. Canizares and F. L. Alvarado, "Point of collapse and continuation methods for large ac/dc systems," *IEEE Transactions on Power Apparatus and Systems*, Vol. 8, pp. 1-8, 1993.

[46] C. W. Taylor, "Concept of Undervoltage Load Shedding for Voltage Stability," *IEEE Transactions on Power Delivery*, Vol.7, No. 2, pp. 480-488, April 1992.

[47] A. Guzman, D. Tziouvara, E. O. Schweitzer, and K. E. Marti, "Load and wide-area network protection system improve power system reliability," *Proceeding of 59th Annual Protective Relaying Conference*, Atlanta, Georgia, April 2005.

[48] L. Sandberg, K. Rouden, and L. Ekstam, "Security Assessment Against Voltage Collapse Based on Real-time Data Including Generator Reactive Power Capacity," *Proc. CIGRE*, 1994.

[49] C. Taylor and R. Ramanathan, "BPA Reactive Power Monitoring and Control Following the August 10, 1996 Power Failure," *Proc. VI SEPOPE*, Salvador, Brazil, May 1998.

[50] C. W. Taylor, "The Future in On-Line Security Assessment and Wide-Area Stability Control," *Proceeding of the 2000 IEEE/PES Winter Meeting*, Vol. 1, January 2000.

[51] F. C. Schweppe and J. Wildes, "Power System Static-State Estimation, Part I: Exact Model," *IEEE Transactions on Power Apparatus and Systems*, Vol. PAS-89, pp. 120-125, January 1970.

[52] F. C. Schweppe and D. B. Rom, "Power System Static-State Estimation, Part II: Approximate Model," *IEEE Transactions on Power Apparatus and Systems*, Vol. PAS-89, pp. 125-130, January 1970.

[53] F. C. Schweppe, "Power System Static-State Estimation, Part III: Implementation," *IEEE Transactions on Power Apparatus and Systems*, Vol. PAS-89, pp. 130-135, January 1970.

[54] A. Abur and A. G. Exposito, Power System State Estimation- Theory and Implementation, Marcel Dekker, Inc. 2004.

[55] IEEE-SE Standard Board, IEEE Standard for Synchrophasors for Power Systems, *IEEE Publications*, March 2001.

[56] R. R. Shoults and W. J. Bierck, Jr. "Buffer system selection of a steady-state external equivalent model for real-time power flow using an automated model for analysis procedure," *IEEE Transactions on Power Apparatus and Systems*, Vol. 3, No. 3, pp. 1104-1111, August 1988.

[57] University of Washington Power System Test Case Achieve, http://www.ee.washington.edu/research/pstca/